



This item was submitted to Loughborough's Institutional Repository (<https://dspace.lboro.ac.uk/>) by the author and is made available under the following Creative Commons Licence conditions.



CC creative commons
COMMONS DEED

Attribution-NonCommercial-NoDerivs 2.5

You are free:

- to copy, distribute, display, and perform the work

Under the following conditions:

 **Attribution.** You must attribute the work in the manner specified by the author or licensor.

 **Noncommercial.** You may not use this work for commercial purposes.

 **No Derivative Works.** You may not alter, transform, or build upon this work.

- For any reuse or distribution, you must make clear to others the license terms of this work.
- Any of these conditions can be waived if you get permission from the copyright holder.

Your fair use and other rights are in no way affected by the above.

This is a human-readable summary of the [Legal Code \(the full license\)](#).

[Disclaimer](#) 

For the full text of this licence, please go to:
<https://creativecommons.org/licenses/by-nc-nd/2.5/>

Large Deformation of Thermally Bonded Random Fibrous Networks: Microstructural Changes and Damage

Farukh Farukh ^(a), Emrah Demirci ^(a), Memiş Acar ^(a), Behnam Pourdeyhimi ^(b), *Vadim V. Silberschmidt ^(a)

a - Wolfson School of Mechanical and Manufacturing Engineering, Loughborough University, UK

b - Nonwovens Cooperative Research Center, North Carolina State University, Raleigh, NC, USA

*Corresponding author's e-mail: V.Silberschmidt@lboro.ac.uk

Tell: +441509227504; fax: +441509227503

Wolfson School of Mechanical and Manufacturing Engineering, Loughborough University, UK

Abstract:

A mechanical behaviour of random fibrous networks is predominantly governed by their microstructure. This study examines the effect of microstructure on macroscopic deformation and failure behaviour of random fibrous networks and its practical implication for optimization of its structure by using finite-element simulations. A subroutine-based parametric modelling approach – a tool to develop and characterise random fibrous networks – is also presented. Here, a thermally bonded polypropylene nonwoven fabric is used as a model system. Its microstructure is incorporated into the model by explicit introduction of fibres according to their orientation distribution in the fabric. The model accounts for main deformation and damage mechanisms experimentally observed and provides the meso- and macro-level responses of the fabric. The suggested microstructure-based approach identifies and quantifies the spread of stresses and strains in fibres of the network as well as its structural evolution during deformation and damage. It Simulations also predict a continuous shift in a distribution of stresses due to structural evolution and progressive failure of fibres.

Keywords: nonwoven; microstructure; deformation; damage; finite element

1. Introduction

A relationship between microstructure and mechanical performance of a nonwoven random fibrous network is the major focus of this study. In the last decade, deformation and damage behaviours of nonwoven has received considerable attention. Experimental studies

on characterisation of nonwovens are mainly focussed on determination of their performance or the micro-mechanisms involved in their deformation and damage [1-8]. Still, these studies can be hardly used for optimisation of a nonwoven network's structure: through they explained the underlying mechanisms of deformation and damage behaviour they could not quantify fractions of fibres participating in load bearing or evolution of microstructure with fabric's extension, due to limitation of experimental setups. Some of experimental studies were focussed on identification of the effect of microstructure on mechanical behaviour of nonwoven networks in terms of strength or extension. Again, there was no information on levels of stresses and strains in individual fibres and changes in microstructure of nonwovens caused by their extension.

Taking into account the difficulties of experimental characterisation of random nonwoven fibrous networks, it can be stated that test-based quantification of performance of this type of materials is not sufficient for comprehensive understanding of their deformation and damage behaviours. One of the main reasons for this is non-trivial linkage between the mechanical behaviour and microstructure and properties of constituent fibres. Numerical simulation is the best way to overcome such limitations of testing approaches, and several studies based on numerical modelling related to deformation and failure of nonwoven networks can be found in the literature. Most of the works in this area have focussed on predicting strength, extension or damage of the fabric under a certain type of loading without any consideration to networks' microstructure and its evolution during their deformation and damage. These studies include the work of Liao and Adnur [9] and Bais *et al.* [10], based on the classical laminate theory, in which nonwoven network is considered to be composed of layers, each containing fibres oriented along a specific direction. In addition, Demirci *et al.* [11-13] introduced a continuum model based on shell elements to predict the deformation behaviour of the fabric. This model is very useful for assessing mechanical performance of nonwoven fabrics but does not provide any information about their structure. A similar type of model was introduced by Ridruejo *et al.* [14], based on a continuum model that included a phenomenological approach for account for damage mechanisms observed experimentally. That model did not mimic the actual microstructure of nonwovens and could not take into account explicitly the related mechanisms involved in deformation and damage.

Recently, Hou *et al.* [15-16] and Sabuncuoglu *et al.* [17-18] suggested finite-element models with explicit introduction of fibres. These models were very efficient in representing the fabric's actual microstructure and its evolution in terms of fibres and distribution of

stresses and strains. However, both of these models were used to predict the deformation behaviour of the nonwoven fabrics without account for their damage.

More recently, a model was developed by Farukh *et al.* [19] to simulate the deformation and damage behaviour of random fibrous nonwoven networks. This finite-element model was based on a parametric modelling technique used to introduce the fibres directly into the model according to their experimentally measured orientation distribution using a specially developed subroutine. The model predicts the deformation and damage responses of a specimen of the nonwoven fabric under external load. A single-fibre failure criterion was introduced into the model to simulate the damage-initiation and -propagation behaviour of nonwovens as a result of progressive failure of fibres. Besides, explicit introduction of fibres into the model helps to simulate the main deformation and damage mechanisms observed experimentally. The model was extensively validated against experimental results [19-20] and information about a spread of stresses and strains in fibres was obtained. The results in this study are given for two principle directions of nonwovens — machine direction (MD) and cross direction (CD) — linked to maximum and minimum strengths of nonwoven fabrics. Here, the model is used to study the evolution in fabric's microstructure in terms of reorientation of fibres and spread in stresses in fibres from the initial un-stretched state up to the onset of macroscopic damage in the nonwoven network. This information is vital for optimisation of the structure of nonwoven networks for better strength and reliability. A special attention is paid to the practical implications of the results obtained from the model.

2. Model for random fibrous nonwoven networks

The finite-element model for simulation of the deformation behaviour of nonwoven networks was developed by the authors following the experimental study on deformation and damage of a nonwoven fabric. In the uniaxial tensile tests of nonwovens, it was observed that fibres start to reorient themselves along the direction of loading thus increasing their participation in load bearing with increase in deformation. As soon as the fibres reached their critical stress or strain threshold they failed resulting in localized damage in form of fracture zones. Further failure of fibres resulted in damage propagation followed by ultimate failure of the fabric [21]. Apparently, strength of the nonwoven fabric is mostly defined by stretching of fibres as resistance to their re-orientation is almost negligible in comparison. Thus, due to preferential orientation of fibres along MD, a considerable re-orientation of fibres occurred in

loading along CD resulting in a rather compliant response of the fabric in this direction as compared to that in MD [22]. Thus, lack of resistance to fibre reorientation as compared to that of their stretching plays a critical role in defining the anisotropic behaviour of nonwovens.

The model was developed to predict the performance of nonwoven fibrous networks while reproducing the main mechanisms involved in their deformation and damage. In the model, fibres were introduced explicitly using a subroutine-based parametric modelling technique. The randomness of orientation of fibres incorporated into the model was based on the orientation distribution function, measured experimentally. In order to reproduce fully the random nature of the studied material, the scatter in material properties of the constituent fibres, obtained in experiments, was also included into the model. Finally, the single-fibre failure criterion in terms of critical stress was included into the model. Additionally, after a dedicated experimental study, the scatter in single-fibre failure parameter was also implemented into the model.

The detailed description of development of the model is given elsewhere [19-20]. Here, only main steps of model development are given for the sake of clarity. The formulation of finite-element model consists of five main stages, performed in a sequence: (i) network generation, (ii) input of geometric properties, (iii) input of material properties, (iv) fibre-failure criteria, and (v) boundary conditions and loading case. These steps are briefly described below.

2.1 Network generation

The process of development of finite-element model was started by the generation of a nonwoven network. It was created by using a discontinuous model with direct introduction of fibres, having, as a result, voids and gaps in it. The material used as a model system in this study was a low-density (20 g/m^2) thermally calendered bonded nonwoven fabric based on polypropylene (PP) fibres (Fig. 1). It was composed of two regions — bond points and fibre matrix — having different microstructure. In order to generate a similar network for the finite-element study, bond points were modelled first, according to their shape, size and pattern in the real fabric; the respective parameters are given in Table 1. Then, the numbers of fibres for bands of orientation angles ranging from 0° to 180° were calculated based on the orientation distribution function (ODF) of fibres in fabric determined from images of the

fabric; the process for obtaining ODF is given in [23]. For defining the numbers of fibres, first the total number of fibres in the model was calculated by using an assumption that the entire fibre mass in the model was equal to that of the sample of the fabric with dimensions equal to those of the model. The fibre mass was calculated by subtracting the mass of the bond points from the fabric mass. The latter was calculated using the following relation:

$$M_{\text{Fabric}} = \rho_{\text{Fabric}} A_{\text{Fabric}},$$

where ρ_{Fabric} is the fabric's planar density (20g/m^2 in this study) and A_{Fabric} is the area of the fabric to be modelled. The mass of bond points (m_{bonds}) was calculated as

$$m_{\text{bonds}} = \rho_{\text{pp}} A_{\text{bond}} t_{\text{bond}},$$

where ρ_{pp} is the density of the constituent fibre material (0.89g/cm^3 in this study), A_{bond} is the total area covered by bond points within the fabric and t_{bond} is the thickness of bond points. The area covered by bond points (A_{bond}) is the product of the modelled fabric's area and a specific area of bond points in the fabric. For this calculation, bond points were considered as continuous regions, following the experimental observations. Then, the total fibre mass was obtained as:

$$m_{\text{Fibre}} = M_{\text{Fabric}} - m_{\text{bonds}}.$$

Finally, the number of fibres to be modelled was calculated by using the following relation:

$$N_{\text{Fibre}} = \frac{m_{\text{Fibre}}}{\rho_{\text{pp}} a_{\text{Fibre}} L_{\text{single_fibre}}},$$

where a_{Fibre} is the cross-sectional area of fibres and $L_{\text{single_fibre}}$ is the length of individual fibres.

This calculation was based on the assumption that fibres lie completely inside the specified fabric region. Since fibres were modelled randomly in the microstructure, characterized with the orientation distribution function, some of the fibres could be located close to the edge of the fabric and parts of them could be outside the modelled region (Fig. 2). For example, a part of fibre B in Fig. 2 is outside the fabric's limits and would be trimmed at later stages of modelling. In order to make the total mass of fibres in the FE model equal to that of the modelled fabric sample, additional fibres were added one by one into the model until both masses became equal. Obviously, there was a small tolerance in mass of the model, which

was less than the mass of the single fibre. The reason for this tolerance is that all the fibres had a constant length, and the last added fibre had some additional resulting in this tolerance. Obviously, its effect is relatively small for a model with a large total number of fibres. The process of model-building was performed virtually, before starting the actual modelling process, to reduce the computation time.

After calculating the number of fibres to be modelled by this virtual modelling process, generation of a random fabric was implemented following the algorithm shown in Fig. 3. The number of fibres for each angle band $N_{\text{Fibre}}(j)$ was defined by the frequency of fibres in each fibre orientation band multiplied by the total number of fibres: The number of truss elements (lines) for each band in the model of the network is then defined as

$$NL(j) = N_{\text{Fibre}}(j)K,$$

where $NL(j)$ is the number of lines having the same orientation as fibres in any particular fibre-orientation band. K is the model coefficient, which is equal to the number of fibres represented by each line (truss element). The value of K ranges from 1 to a certain higher value depending on the computational efficiency of the system used for simulations. If it is low, and a higher value of the model coefficient K is used, the geometric properties related to fibre should be updated respectively. For example, if $K = 9$ is used, the diameter of the truss element should be three times the diameter of a single fibre. Historically, models with $K > 1$ were developed (e.g. [24, 25]), with each truss element representing several fibres. These models predicted the macroscopic response of a nonwoven material but did not consider damage development or structural evolution of networks. Still, the use of $K = 1$ can be impractical (or even infeasible) in models with very large total numbers of fibres; in such cases $K > 1$ is the way to implement the simulations. All calculations of the numbers of fibres for particular fibre orientation bands were performed by the special subroutine based on the input parameters characterising the fabric before modelling the fibres; it reduces the time to generate the model with a large number of fibres. The flow chart of calculating and modelling of number of fibres is shown in Fig. 3. The software used for this purpose was MSC. Patran. Since the nonwoven network in this study was anisotropic with preferential orientation of fibres along the machine direction (MD), therefore, two models with dimensions 16.5 mm gauge lengths along MD and CD (the width in both cases was 10 mm) were developed using the subroutine to study anisotropic mechanical behaviour of the nonwoven under study. The

choice of model dimensions was to optimise, on the one hand, computational efforts of models with large numbers of fibres and, on the other hand, representativeness of the fabric's microstructure with its features.

2.2 Geometric and material properties

Bond points were modelled with shell elements (element type 139 in MSC.Marc), while fibres were modelled with truss elements (element type 9 in MSC. Marc), which have only axial stiffness. Since truss elements cannot carry any bending moment, they were appropriate to represent fibres characterised by a rather low flexural stiffness. Thickness of bond points (0.0337 mm) and diameter of single-fibre (0.018 mm), corresponding to the model coefficient $K = 1$, were assigned to the corresponding elements.

The material properties of constituent fibres obtained in experimental studies were introduced directly into the model, since fibres were modelled explicitly. These properties were obtained with tests on single fibres extracted from the fabric: elastic-plastic properties — from single-fibre tensile tests and viscous ones — from single-fibre creep tests. The complete details of these single-fibre experiments can be found elsewhere [19, 20]; some of the properties are given in Table 2. For the elastic region, the stress-strain relation was given as

$$\sigma^e = E\varepsilon^e, \quad (1)$$

where E is the Young's modulus. Using the flow stress definition with table-based input, the hardening slope at each increment was obtained by numerical differentiation of the values in the table; these values were based on a plot of the stress versus plastic strain for a tensile test. The generalized form of the work-hardening coefficient has the following form:

$$H = \frac{d\bar{\sigma}}{d\bar{\varepsilon}^p}, \quad (6)$$

where $d\bar{\varepsilon}^p$ and $d\bar{\sigma}$ are equivalent plastic strain and equivalent stress. The flow rule, describing changes in plastic strain component as a function of the current stress state, essential to define the incremental stress-strain relation for plastic material, can be expressed as:

$$d\varepsilon^p = d\bar{\varepsilon}^p : \nabla \bar{\sigma} \quad (7)$$

where

$$\nabla \bar{\sigma} = \frac{\partial \bar{\sigma}}{\partial \sigma_{ij}}$$

It can be shown (MSC. Marc, 2013) that by rearranging

$$d\bar{\varepsilon}^p = \frac{\nabla \bar{\sigma} : C : d\varepsilon}{H + \nabla \bar{\sigma} : C : \nabla \bar{\sigma}}, \quad (8)$$

where C is the stiffness matrix.

The scatter in material properties was implemented into the model by means of sets of fibres with different material properties. The numbers of fibres in each set with certain material properties were assigned according to the statistics of experimental observations; in total, seven fibre sets were used in the model. The material properties of constituent fibres were introduced into the model based on assumption that their cross-section was perfectly circular and the diameter is constant throughout its length. True-stress and true-strain values were computed based on a hypothesis that deformation in fibres took place at a constant volume. The median values of basic mechanical properties of fibres are given in Table 2. Some of the average properties such as density and melting point were obtained from the data provided by the manufacturer, i.e. FiberVisions, USA.

2.3 Fibre-failure criterion

In stretched thermally bonded nonwovens, fibres reorient themselves along the direction of loading and start participating in load bearing. They fail on reaching their stress or strain threshold resulting in damage initiation. This process of fibre failures continues until failure of the fabric occurs. Explicit introduction of fibres into the model makes it possible to characterise the changes in network's topology depending on deformation and progressive failure of fibres.

Single-fibre critical stress values were obtained by performing tensile tests on fibres extracted from the fabric in a way that they were attached to bond points at each end; the details of the experiments are given in [26]. These experiments provided the values of

strength of fibres in the real fabric that was affected by the manufacturing process. The measured scatter in failure stress of fibres was included into the model; the values of fibres' failure stresses with their frequency for seven sets used in the FE model are given in Table 3. In the FE model, a fibre was assumed to fail during deformation when the respective failure condition was satisfied (i.e. the stress level in fibre attained its failure stress). The element was removed from the model when this condition was fulfilled to avoid the convergence problem. Since the fabric, used in this study, was bonded at optimal conditions, there were no failures of bond points. Following this experimental observation, no failure criterion was implemented for bond points. The average Young's modulus obtained from single-fibre tensile test was used for the shell elements modelling the bond points.

2.4 Boundary conditions and load case

Boundary conditions in FE analysis allow a direct link between the simulation and the respective real-life problem as they represent loads and constraints of the real-life case. The boundary conditions of uniaxial deformation were applied in models of deformation in MD and CD (Fig. 6). The strain rate of 0.1 s^{-1} was applied on nodes on one end of the model whereas its other end was fully fixed. Since any lateral displacements were also not possible in the grips of the testing machine, the transverse degree of freedom of the respective nodes in the model were constrained. Under these conditions, simulations were carried out for 200% of fabric's extension.

3. Experimental validation

Rectangular specimens of the nonwoven network cut along MD and CD with dimensions 16.5 mm by 10 mm were tested in tension using the cut-strip test method. The schematics of the sample are shown in Fig. 4. The ends of the specimen between the grips with rubber inside were restricted with regard to lateral contraction. The tensile tests were carried out at strain rate of 0.1 s^{-1} . Further details about the experimental setup can be found in [21].

The global shapes of the specimens deformed to high strains for both CD and MD shown in Fig. 6 are similar to hour-glass. This shape, typical for specimen with constrained lateral contraction, was more prominent in the specimen stretched along MD than CD during the initial stages of the experiments due to the preferential orientation of fibres.

The results of simulations were compared with the experimental data with regard to force-displacement curves as shown Fig. 7. The curves obtained from simulations overestimate a response of the stretched fabric at the initial stages of its deformation for both directions. Still, the simulated curves are in a good agreement with the experimental ones both for MD and CD. The only difference between experimental and simulation results is the extent of scatter, which is greater in the former case. In simulations, three parameters define randomness in of the modelled material: orientation distribution of fibres, their position in the network and their material properties as shown in Fig. 5. The fibre positions in network and the bands of particular material properties were assigned using the random-number generator (RNG). Obviously, using different orientation distributions of fibres and assigning different sets of random numbers for position and properties of fibres would give a rise to a scatter in simulation results for multiple statistical realizations similar to that for experimental observations. In order to gain a better understanding of the scatter that can be obtained in simulation, another model with different seeds for RNG for the fibres with the same ODF was developed. The rest of simulation parameters including sets of single-fibre material properties, their failure criterion and boundary condition remained the same for direct comparison. The simulation results in terms of force-extension graph are presented in Fig. 7 with continuous lines. The graph shows that variation only in one of the modelling parameters gives scatter in results; the overall shape of force-extension curve — characterised by a long tail in MD and a sudden drop in CD after the maximum level of network's strength — remained the same.

In order to examine the predictive capability of the model, another model – with dimensions 16.5 mm (gauge length) \times 5 mm (width) in MD – was prepared. All other parameters remained the same. The results obtained from the simulation in terms of force-extension curve are shown in Fig. 8 and compared with experimental data for the corresponding sample dimensions. By comparing Figs. 7 and 8, it was observed that the fabric's response was directly affected by the sample's size and the developed FE model is capable to predict that variation in results.

4. Non-uniform stress distribution

The developed parametric finite-element model was used to obtain distributions of stresses and strains in the nonwoven network. Explicit introduction of fibres into the model allows predictions of the level of stresses and strains in each element (fibre in this case) of the

model. Since fibres were modelled randomly, according to the ODF measured for the real fabric, and their participation in the load-bearing process changed as they were aligned along the loading direction with stretching of the network, the levels of strain (ϵ_f) in each fibre could deviate from the global strain in fabric ($\bar{\epsilon}$) depending upon its orientation with respect to the loading direction and its position in the network. Respectively, the stress levels in fibres (σ_f) were randomly distributed in the modelled specimen at any stage of deformation; this can be observed in Fig. 6.

Due to a large number of fibre elements involved the simulations (truss elements in model in Fig. 6), a special Python code was developed to acquire the level of stress in each fibre. The calculated data for stress distributions in fibres for MD and CD with respect to fabric's extension are shown in Fig. 9 in the form of percentile bands. Since most of the fibres failed at global strain of 100% in MD, therefore, the results in Fig. 9 are shown up to this level of fabric's extension. In Fig. 9, each band presents ten percentile ranks of fibres. For MD (Fig. 9a), stresses in all the fibres increased up to strain of 50%. With further extension, some 80 percent of fibres tend to return to their unstressed state due to progressive failure of fibres. Thus, after fabric's extension by 50% only 20% of its fibres transfer the load with the rest of the fibres regaining their original unstressed state due to formation of fracture zones. Since progressive failure of fibres resulted in a continuous transfer of load to the neighbouring elements, a sudden increase in stresses in remaining 20% of fibres bearing load for MD was observed (Fig. 9a). For CD (Fig. 9b), a continuous increase in stresses in fibres shows a growing extent of participation in load bearing. Apparently, the gradual increase in stresses in fibres for CD as compared to that of for MD is a result of large reorientation of fibres taking place before their participation in load bearing for CD, which is consistent with the observed ODF. Due to rotation of the fibres during fabric's extension, the orientation distribution function changes continuously. The developed model is capable to capture the continuously varying orientation distribution function as shown in Fig. 10 that provides a comparison between the initial ODF and the one for fabric's extension of 50% in MD. Since the developed model provides information on fibres participating in load bearing at any level of fabric's extension, it can be used as a tool for optimisation of the structure of nonwoven networks in terms of orientation distribution of fibres to improve its strength and robustness. This can be achieved by arranging the fibres in a network in a way that more uniform stress and strain distributions are obtained. Since the model was developed using the subroutine-

based parametric modelling technique, it can significantly reduce the effort required for reformulation of the model necessary to study different network topologies.

5. Quantitative analysis of structural evolution

The developed Python code was also used to obtain the information about reorientation of fibres in the stretched fabric. The evolution of ODF presented in Fig. 10 can be additionally quantified by introduction of a measure of average reorientation of fibres with increasing levels of fabric's extension. The respective results for loading along both directions — MD and CD — are given in Fig. 11. This parameter was calculated by subtracting the average of absolute values of fibres' angles with the loading axis for the given stage of deformation from that for the initial, unloaded stage:

$$\langle \Delta \theta \rangle = |\theta_i|_{\text{avg}} - |\theta_f|_{\text{avg}}.$$

The reason behind using the absolute values of angles is to get the net reorientation angle whether it is in a clockwise or an anti-clockwise direction. The comparison with the initial orientation of fibres provides information about evolution of the fabric's microstructure with its extension. For CD (Fig. 11), the continuous increase in re-orientation of fibres was observed as a result of constant evolution of the fabric's network structure with the increasing level of its extension. For MD (Fig. 11), in contrast, reorientation of fibres was observed up to fabric's extension of 50%. After this level of extension, formation of failure zones was accompanied by parts of the fabric regaining their initial un-stretched form. This caused the remaining fibres to reorient towards their initial orientation, i.e. the state when no load was applied. However, fibres did not fully regain their initial orientation, demonstrating permanent deformation of the fabric similar to that observed experimentally. Thus, the model is capable to predict the changes in the network's structural evolution with its extension, which can be used to assess the life in service for a nonwoven network in terms, e.g., of loading cycles. Besides, it can provide information on the maximum load-carrying capacity or allowable extension of the nonwoven network before damage initiation; thus, it can be used to introduce the safety factor for products containing nonwoven parts.

6. Conclusions

The mechanical performance of polypropylene-based thermally bonded nonwoven fibrous network was studied by employing a specifically developed finite-element model. A novel

method based on the parametric modelling technique was used to develop the model. The fibres were introduced directly into it according to their ODF obtained from the SEM images of the fabric using the image analysis technique. This microstructure-based numerical approach maintains a relation between a microstructure of the studied nonwoven fibrous network and its deformation and damage behaviours. All the parameters necessary for simulation of such a fibrous network, including the orientation distribution function for fibres, geometric properties, material properties, failure criteria as well as the shape, size, dimensions and pattern of bond points were obtained from the experiments performed with single fibres and fabrics specimens [19-21]. The model developed in this study can predict the character of evolution of deformation and damage of the fabric up to its failure in terms of progressive failure of fibres. Thanks to explicit introduction of fibres into the model, it provides the data for a spread of stresses and strains in elements of the network, reorientation of the fibres, and fraction of fibres taking the load for any level of fabric's extension.

The model shows that for this particular ODF, biased towards MD, extensive rotation of fibres occurred for loading in CD as compared to that in MD. Moreover, only 20% fibres took part in load-bearing after extension of fabric by 50% in MD whereas the rest of the fibres started reorienting to regain their original position. However, in CD, continuous rotation of fibres occurred until it reached the maximum value followed by failure of the fabric. Thus, the model was capable to predict the structural evolution of fabric in terms of reorientation of fibres.

Since the model can also predict the stress level for each element of the fibrous network, it can help to find out the areas where the damage will initiate for arbitrary loading conditions. Hence, this model can provide an important set of information about nonwoven networks, which cannot be obtained easily with the existing models or from the experiments. Since fibres are explicitly introduced into the model, which reproduces reorientation in the direction of loading on deformation and changes in participation in the load-bearing process, the model can be extended to study the deformation and damage behaviour of random fibrous nonwoven networks under bi-axial loading as performed in [27] or arbitrary multi-stage loading regimes. Thus, it can be used by a designer and a manufacturer of nonwovens to determine performance and safety factor of products containing nonwoven networks. Moreover, the failure locus with a number of fibres failed at any level of nonwoven network's extension can be predicted using this model.

Acknowledgement

We greatly acknowledge support by the Nonwovens Cooperative Research Centre of North Carolina State University, Raleigh, USA. FiberVisions®, USA generously provided the material for this study.

References

- [1] Ridruejo A, Gonzalez C, Llorca J (2011) Micromechanisms of deformation and fracture of polypropylene nonwoven fabrics. *Int J Solids Struct* 48:153-162.
- [2] Kim HS, Pourdeyhimi B (2000) Characterization of structural changes in nonwoven fabrics during load-deformation experiments. *J Text Appar Tech Manag* 1
- [3] Farukh F, Demirci E, Acar M, Pourdeyhimi B, Silberschmidt VV (2013) Meso-scale deformation and damage in thermally bonded nonwovens. *J Mater Sci* 48:2334-2345.
- [4] Kim HS (2004) Relationship between fiber orientation distribution function and mechanical anisotropy of thermally point-bonded nonwovens. *Fibers Polymer* 5:177–181.
- [5] Kim HS, Pourdeyhimi B (2001) The role of structure on mechanical properties of nonwoven fabrics. *Int Nonwovens J* 10:32–37.
- [6] Michielsen S, Pourdeyhimi B, Desai P (2006) Review of thermally point-bonded nonwovens: materials, processes and properties. *J Appl Polymer Sci* 99:2489-2496.
- [7] Bhat G S, Jangala PK, Spruiell JE (2004) Thermal bonding of polypropylene nonwovens: effect of bonding variables on the structure and properties of the fabric. *J Appl Polymer Sci* 92:3593-3600.
- [8] Keller DS, Branca DL (2012) Characterization of nonwoven structures by spatial partitioning of local thickness and mass density. *J Mat Sci* 47:208-226.
- [9] Liao T, Adanur S, Drean JY (1997) Predicting the mechanical properties of nonwoven geotextiles with the finite element method. *Textile Res J*, 67 753-760.
- [10] Bias-Singh S, Anandjiwala RD, Goswami BC (1996) Characterizing lateral contraction behavior of spunbonded nonwovens during uniaxial tensile deformation. *Textile Res J* 66: 131-140.
- [11] Demirci E, Acar M, Pourdeyhimi B, Silberschmidt VV (2011) Dynamic response of thermally bonded bicomponent fibre nonwovens. *Appl Mech Mater* 70:410-415

- [12] Demirci E, Acar M, Pourdeyhimi B, Silberschmidt VV (2011) Finite element modelling of thermally bonded bicomponent fibre nonwovens: tensile behaviour. *Comput Mater Sci* 50:1286-129.
- [13] Demirci E, Acar M, Pourdeyhimi B, Silberschmidt VV (2010) *ASME Conf Proc; ESDA2010*: 117-122
- [14] Ridruejo A, Gonzalez C, LLorca J (2012) A constitutive model for the in-plane mechanical behavior of nonwoven fabrics. *Int J Solids Struct* 49:2215-2229.
- [15] Hou X, Acar M, Silberschmidt VV (2011) Finite element simulation of low-density thermally bonded nonwoven materials: effect of orientation distribution function and arrangement of bond points. *Comput Mater Sci* 50:1292-1298.
- [16] Hou X, Acar M, Silberschmidt VV (2011) Non-uniformity of deformation in low-density thermally bonded nonwoven material: effect of microstructure. *J Mater Sci* 46:307-315.
- [17] Sabuncuoglu B, Acar M, Silberschmidt VV (2012) A parametric finite element analysis method for low-density thermally bonded nonwovens. *Comput Mater Sci* 52:164-170.
- [18] Sabuncuoglu B, Acar M, Silberschmidt VV (2013) Parametric code for generation of finite-element model of nonwovens accounting for orientation distribution of fibres. *Int J Numer Meth Engng* 79:143-158.
- [19] Farukh F, Demirci E, Sabuncuoglu B, Acar M, Pourdeyhimi B, Silberschmidt VV (2012) Numerical modelling of damage initiation in low-density thermally bonded nonwovens. *Comput Mater Sci* 64:112-115.
- [20] Farukh F, Demirci E, Sabuncuoğlu B, Acar M, Silberschmidt VV, Pourdeyhimi B (2013) Characterisation and numerical modelling of complex deformation behaviour in thermally bonded nonwovens. *Comput Mater Sci* 71:65-171.
- [21] Farukh F, Demirci E, Acar M, Pourdeyhimi B, Silberschmidt VV (2013) Meso-scale deformation and damage in thermally bonded nonwovens. *J Mat Sci* 48:2334-2345.
- [22] Jearanaisila W P (2008) A continuum model for needlepunched nonwoven fabrics. PhD thesis, MIT, USA.

- [23] Demirci E, Acar M, Pourdeyhimi B, Silberschmidt VV (2012) Computation of mechanical anisotropy in thermally bonded component fibre nonwovens. *Comput Mater Sci* 52:157-163.
- [24] S. Limem, S.B. Warner, Adhesive point-bonded spunbond fabrics, *Textile Res. J.* 75 (1) (2005) 63–72.
- [25] D.H. Mueller, M. Kochmann, Numerical modeling of thermobonded nonwovens, *Int. Nonwovens J.* 13 (1) (2004) 56–62.
- [26] Farukh F, Demirci E, Acar M, Pourdeyhimi B, Silberschmidt, VV (2012) Strength of fibres in low-density thermally bonded nonwovens: An experimental investigation, *J Phys: Conf Series*, 382(012018), <http://dxdoiorg/101088/1742-6596/382/1/012018>.
- [27] Ridruejo A, Gonzalez C, LLorca J (2012) Damage localization and failure under biaxial loading in glass-fibre nonwoven felts. *Int J Multiscale Comp Engg* 10:425-440.

Figure Captions

Figure 1. Microscopic image of thermally bonded nonwoven

Figure 2. Introduction of fibres in the model: fibre A, having a free end in the fabric; fibre B, inside the domain (dashed lines represents model's boundary)

Figure 3. Flow chart of subroutine to generate nonwoven fibrous network

Figure 4. Cut-strip test method used for fabric testing

Figure 5. Sources of scatter in simulation results

Figure 6. Experimental (right) and simulation (left) results (von Mises stress in MPa) for deformed nonwoven after 75% extension in MD (a) and CD (b)

Figure 7. Numerical and experimental force-extension curves of rectangular specimens subjected to tensile loading along MD (a) and CD (b)

Figure 8. Numerical and experimental force-extension curves for specimens of 5 mm width subjected to tensile loading along MD

Figure 9. Distribution of stresses of fibres for various levels of fabric's extension: (a) MD; (b) CD

Figure 10. Orientation distributions of fibres for initial state and at 50% extension of fabric in MD

Figure 11. Rotation of fibres with increasing fabric's extension for MD and CD

Table 1. Parameters of geometry and patterns of bond points

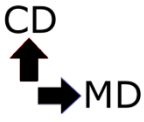
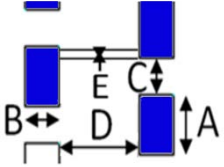
Fabric's orientation with reference to BP	BP pattern	A	B	C	D	E
		(mm)				
		1.0668	0.5588	0.7	1.8	0.2

Table 2. Some properties of polypropylene fibres extracted from nonwoven fabric

Density (g/cm ³)	Young's modulus (MPa)	Poisson's ratio	Yield stress (MPa)	Melting point (°C)
ρ	E	ν	-	-
0.89	350	0.42	75 ± 9	165

Table 3. Failure stresses of polypropylene fibres extracted from nonwoven fabric and their respective frequencies

Set number	Failure stress, MPa	Frequency, %
1	275	10
2	290	20
3	300	10
4	310	10
5	325	20
6	350	20
7	375	10

Figure 1 colour
[Click here to download high resolution image](#)

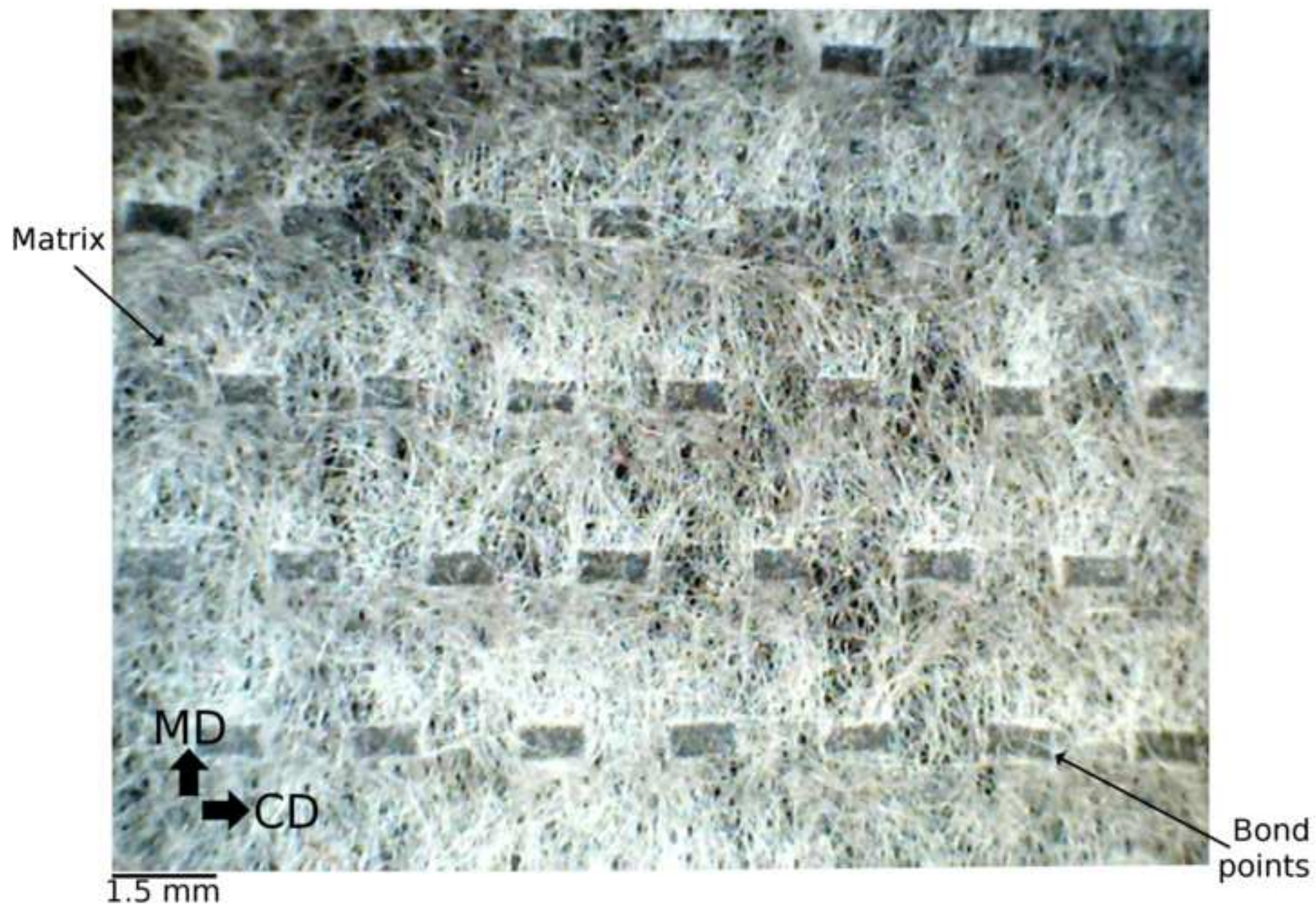


Figure 1 b&w
[Click here to download high resolution image](#)

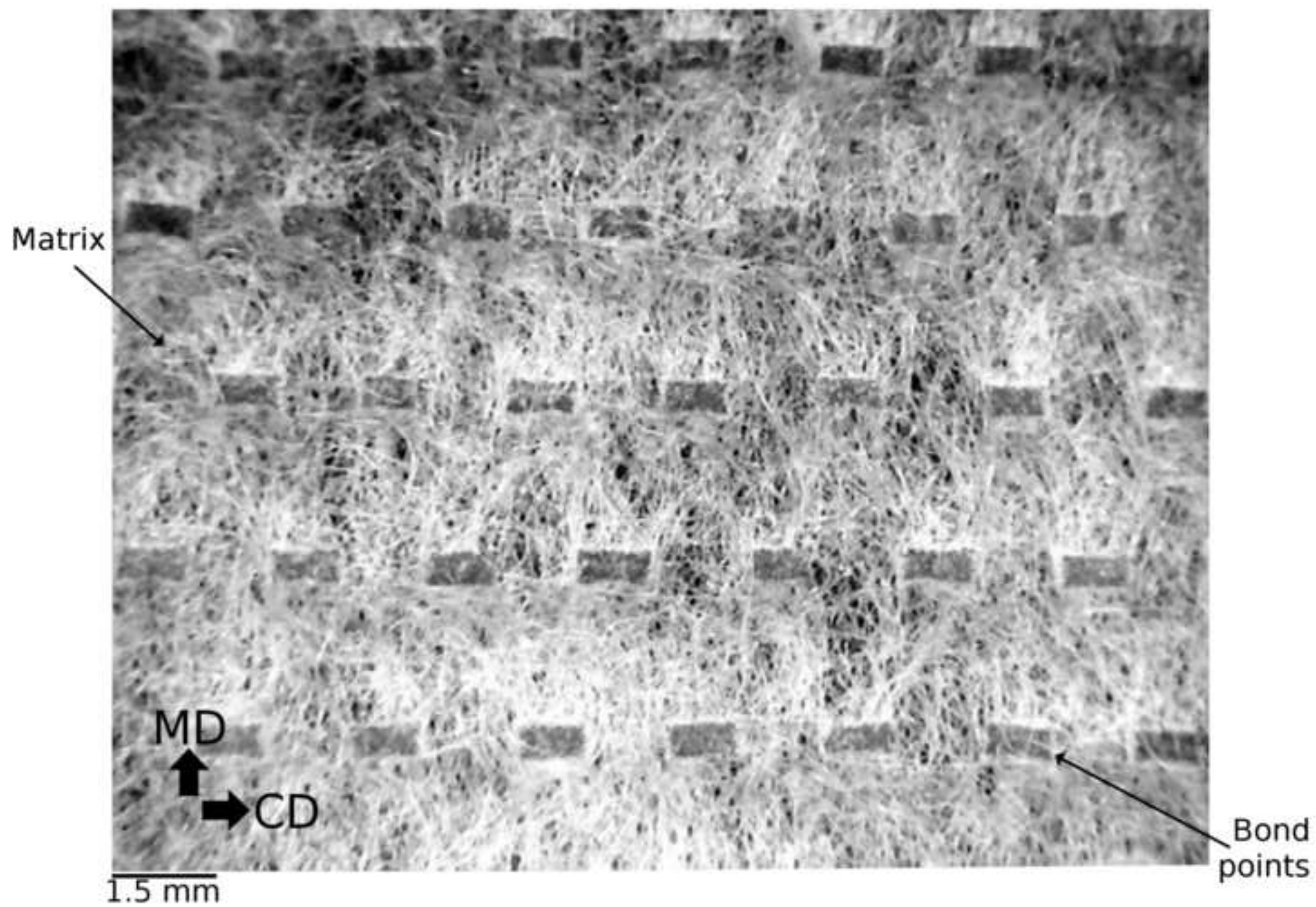


Figure 2
[Click here to download high resolution image](#)

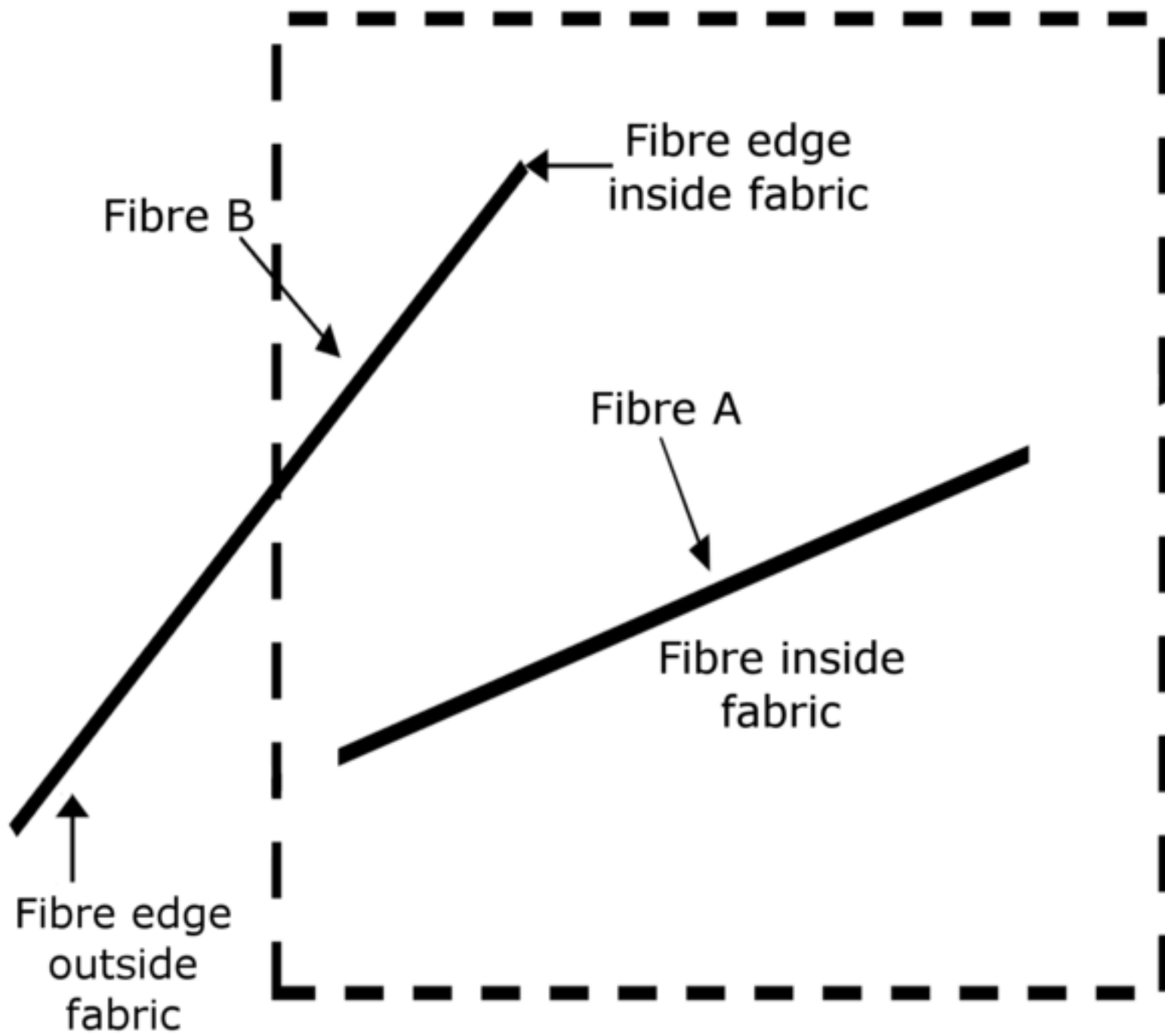


Figure 3
[Click here to download high resolution image](#)

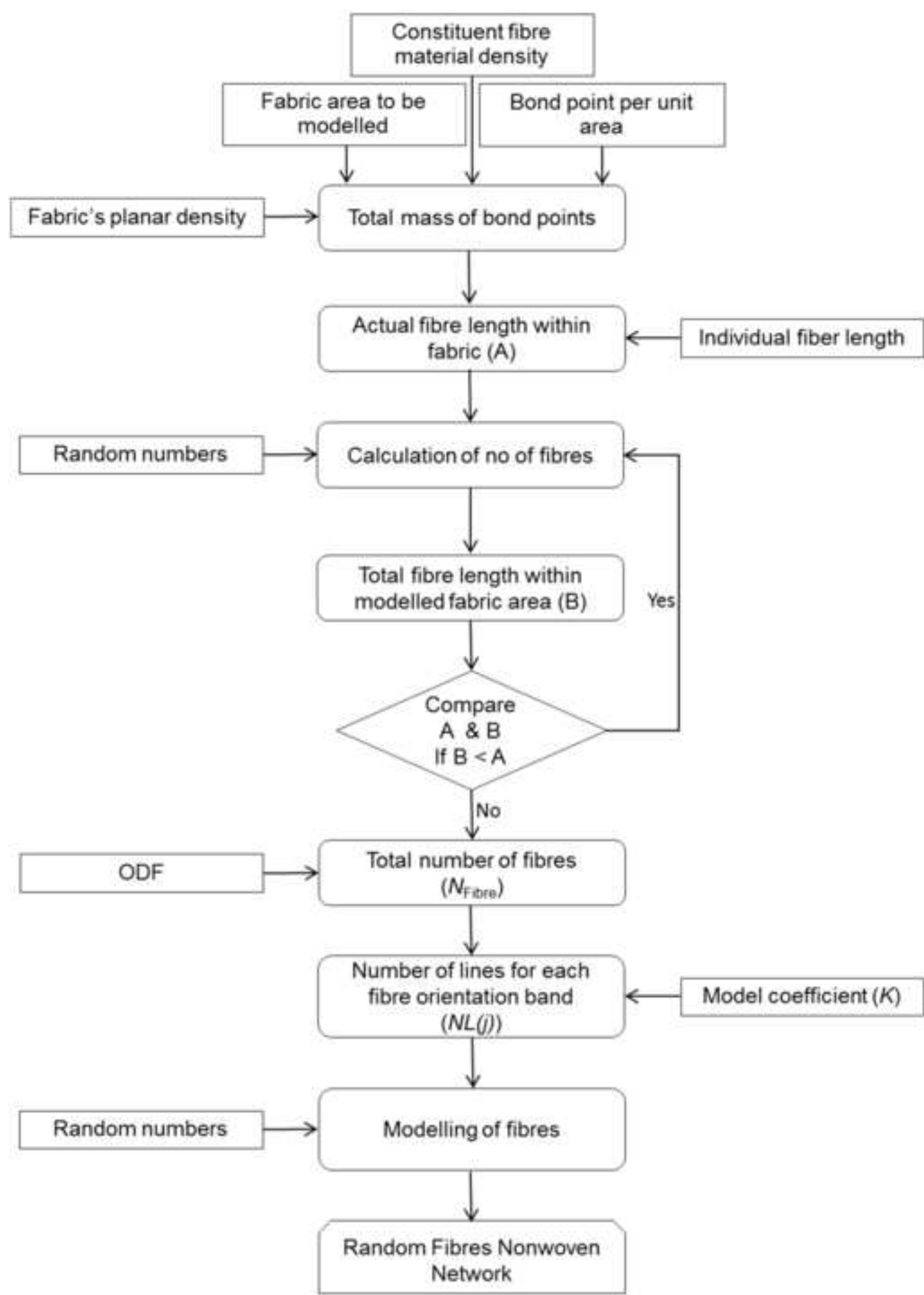


Figure 4
[Click here to download high resolution image](#)

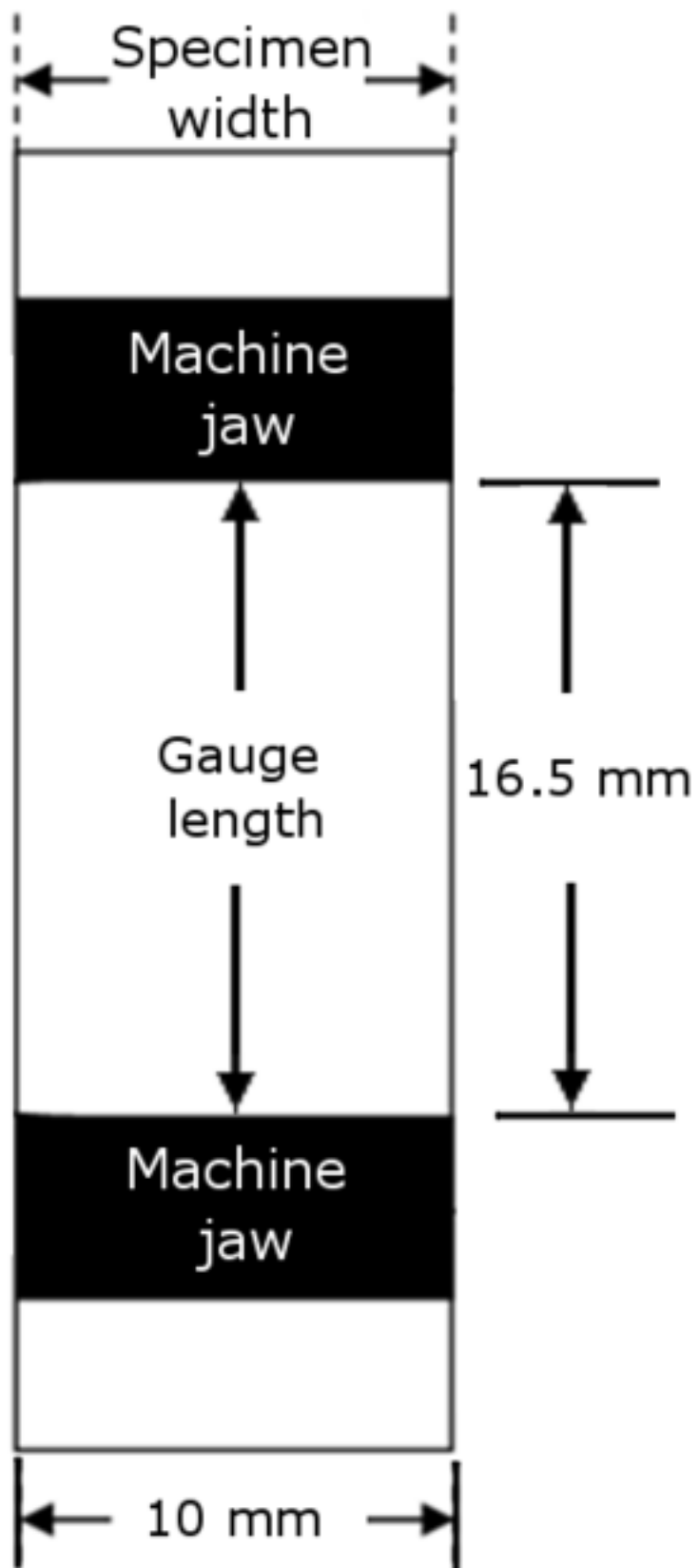


Figure 5
[Click here to download high resolution image](#)

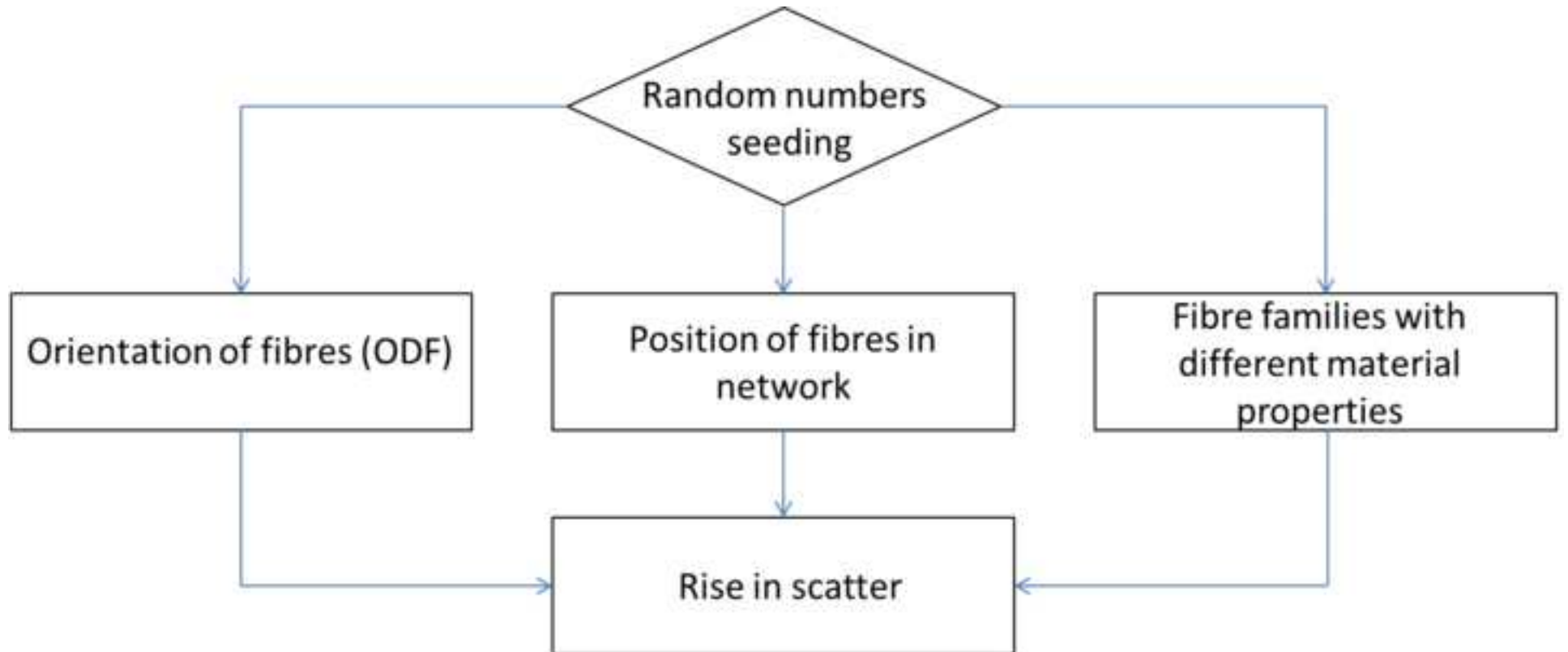


Figure 6a colour
[Click here to download high resolution image](#)

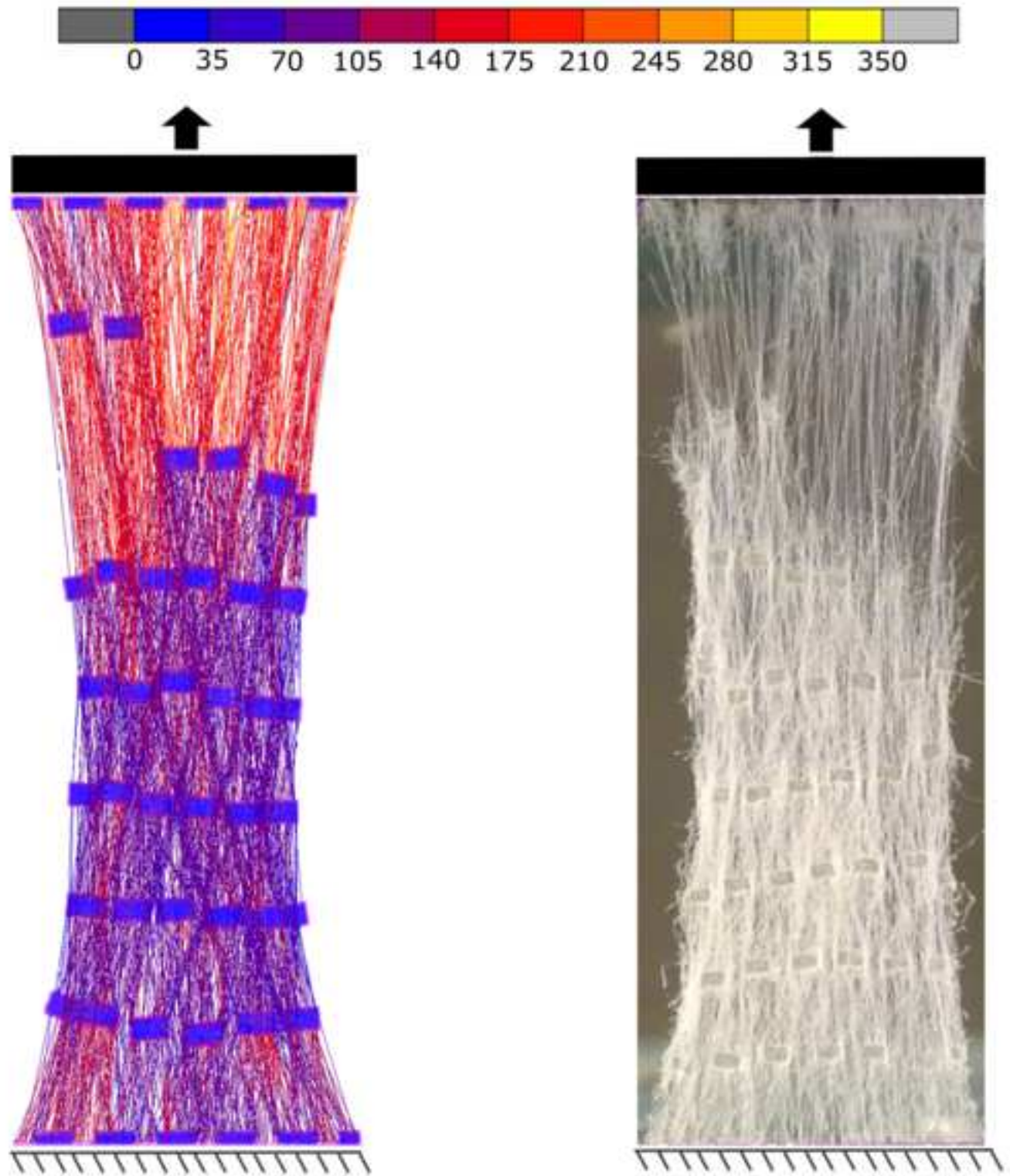


Figure 6b b&w
[Click here to download high resolution image](#)

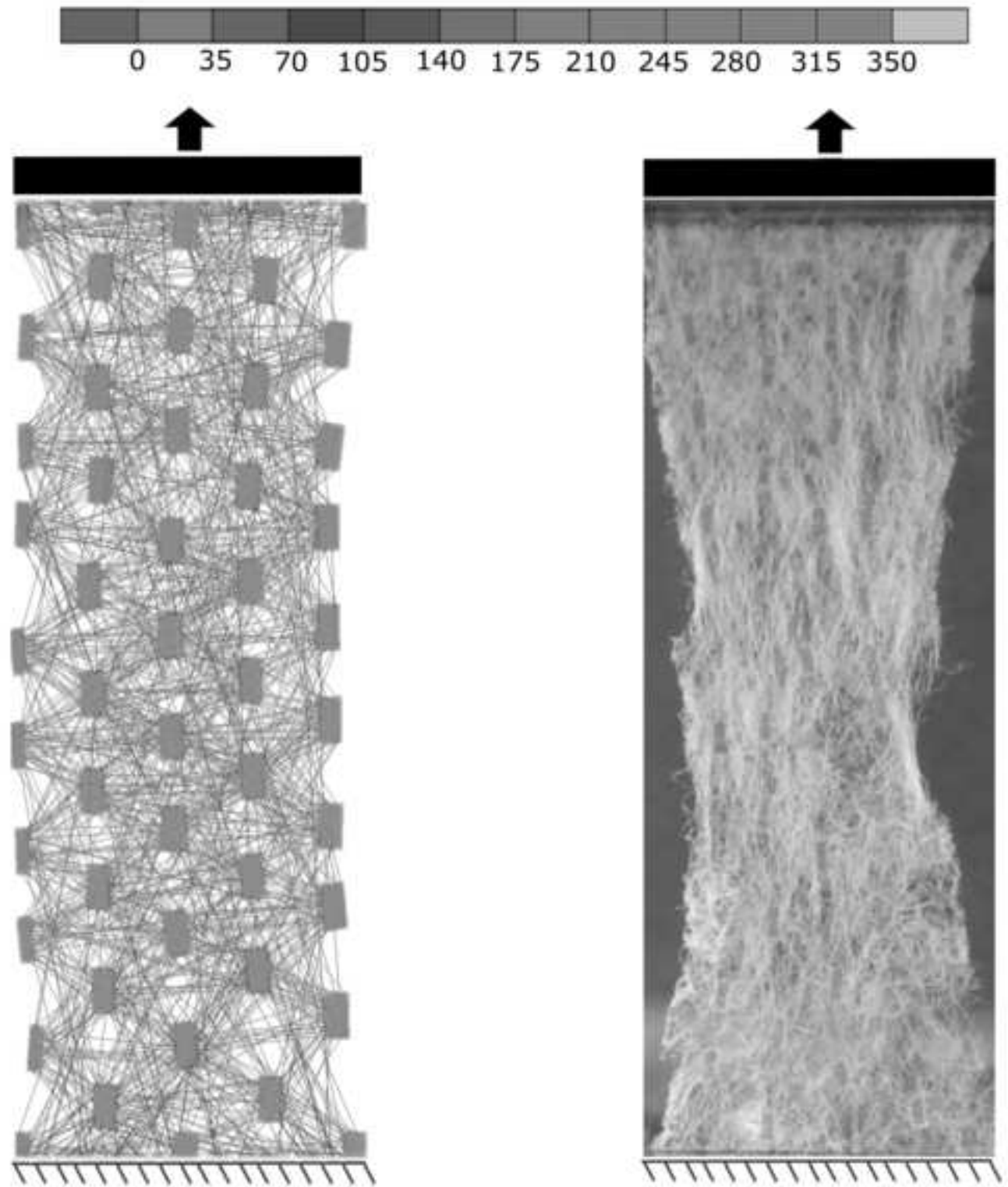


Figure 6b colour
[Click here to download high resolution image](#)

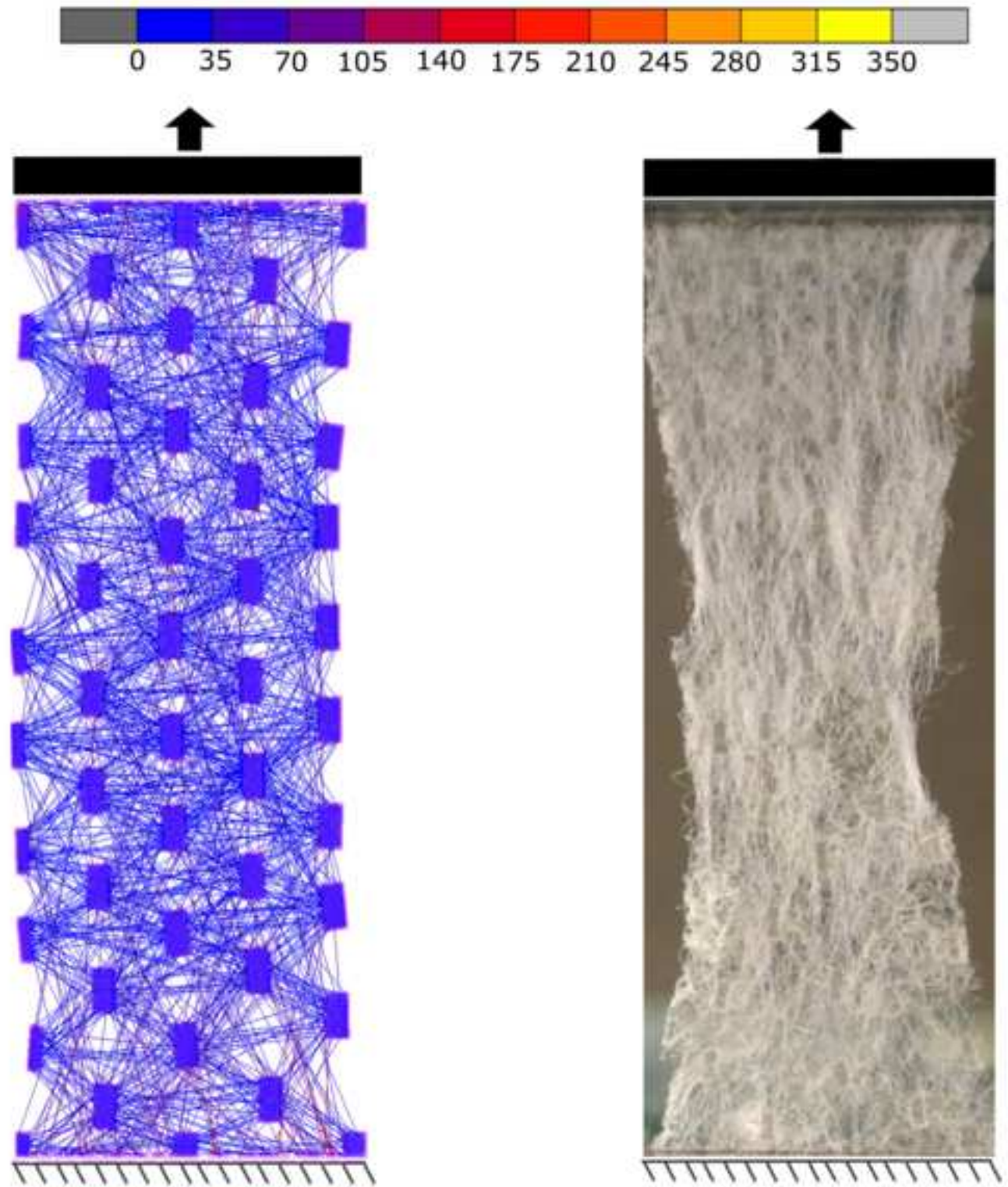


Figure 6a b&w
[Click here to download high resolution image](#)

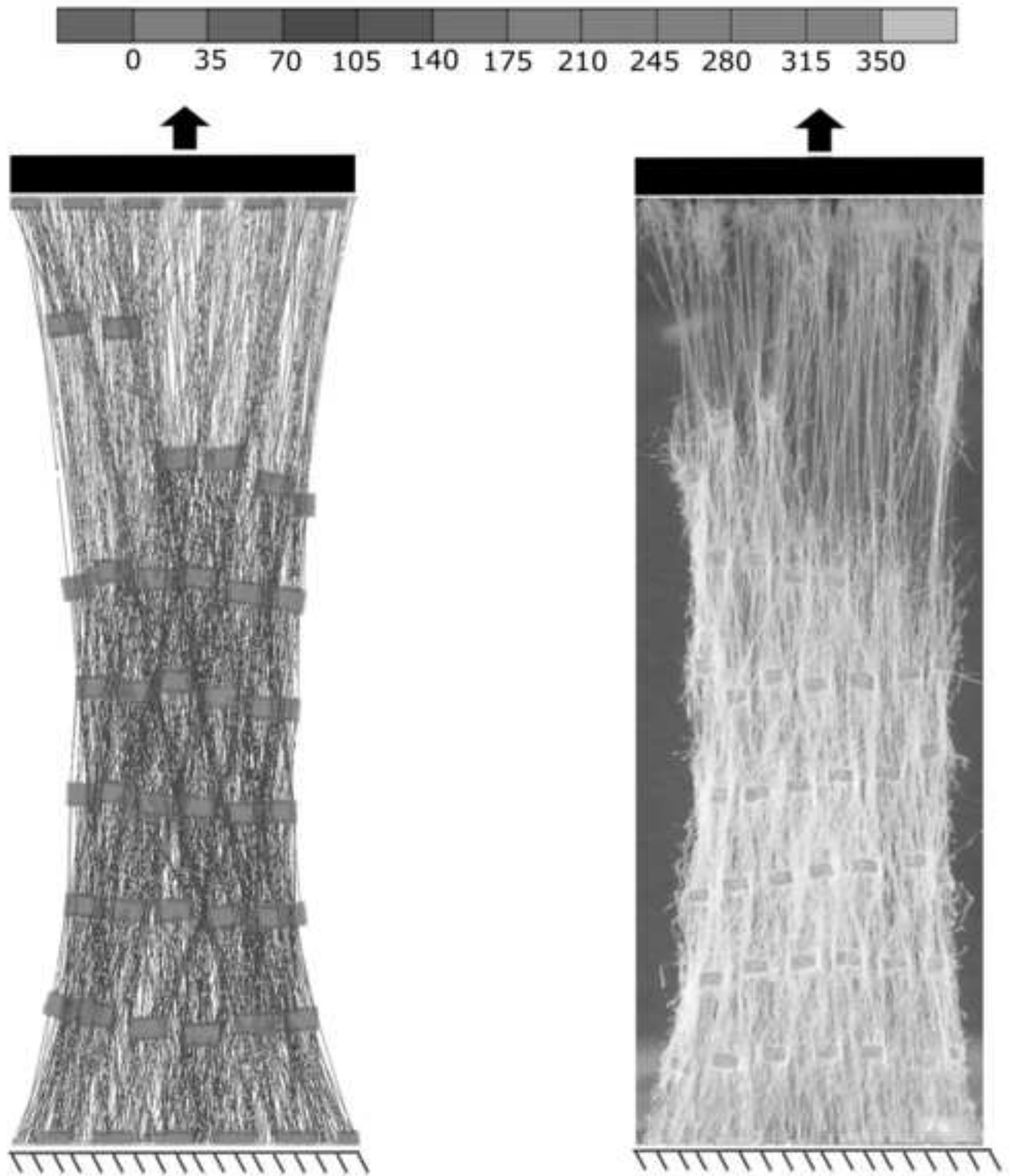


Figure 7a revised colour
[Click here to download high resolution image](#)

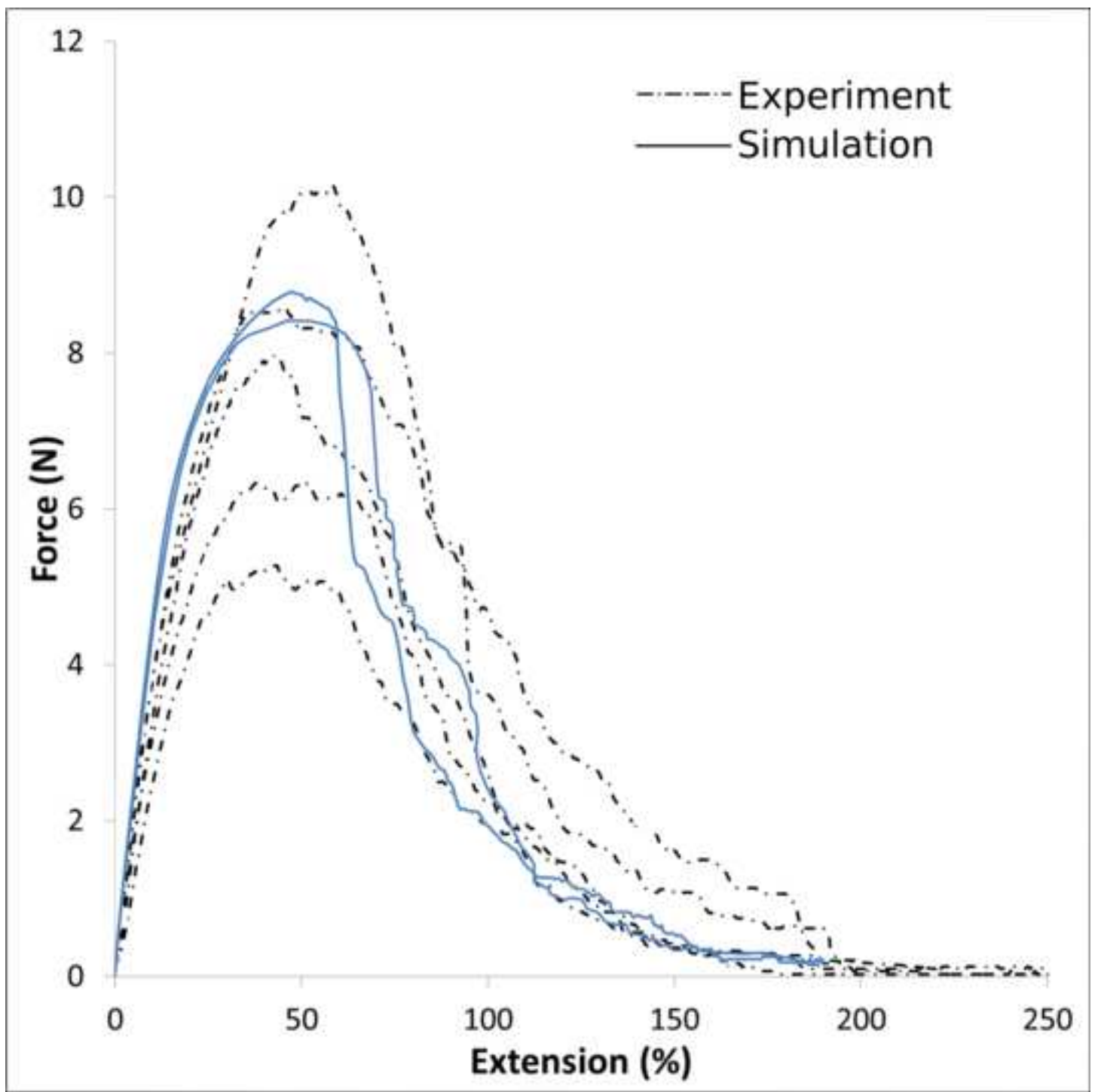


Figure 7a revised b&w
[Click here to download high resolution image](#)

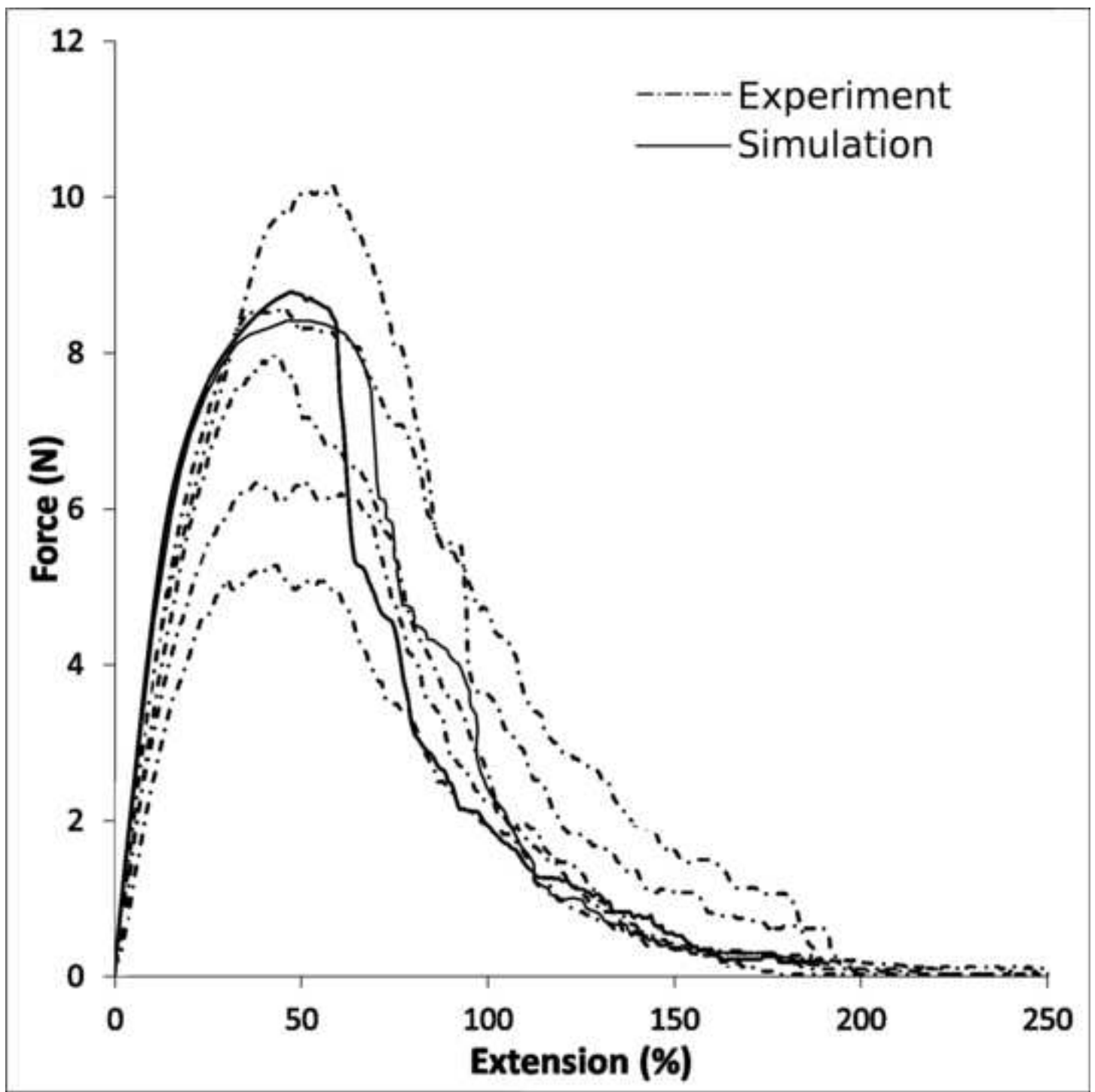
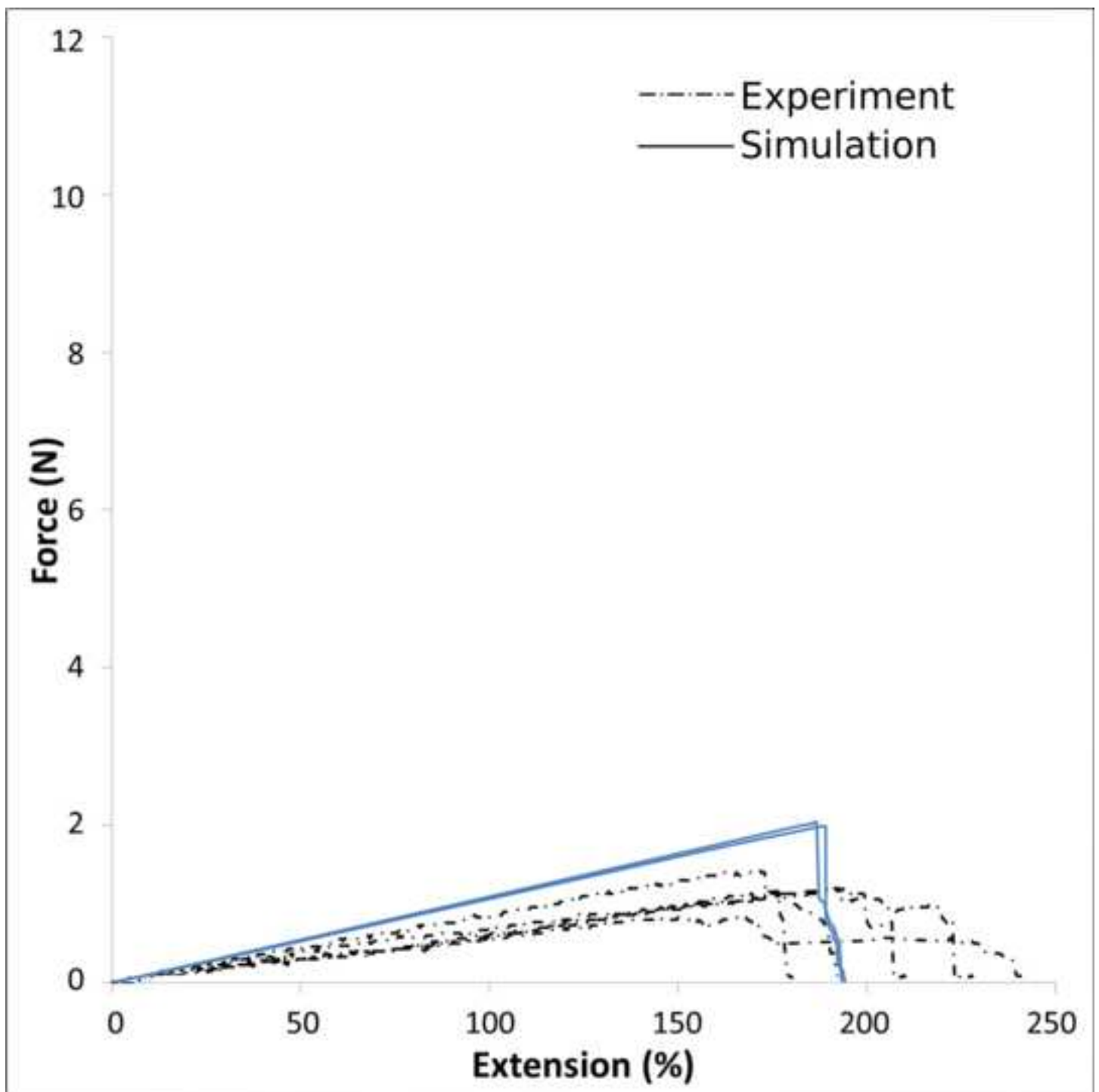


Figure 7b revised bcolour
[Click here to download high resolution image](#)



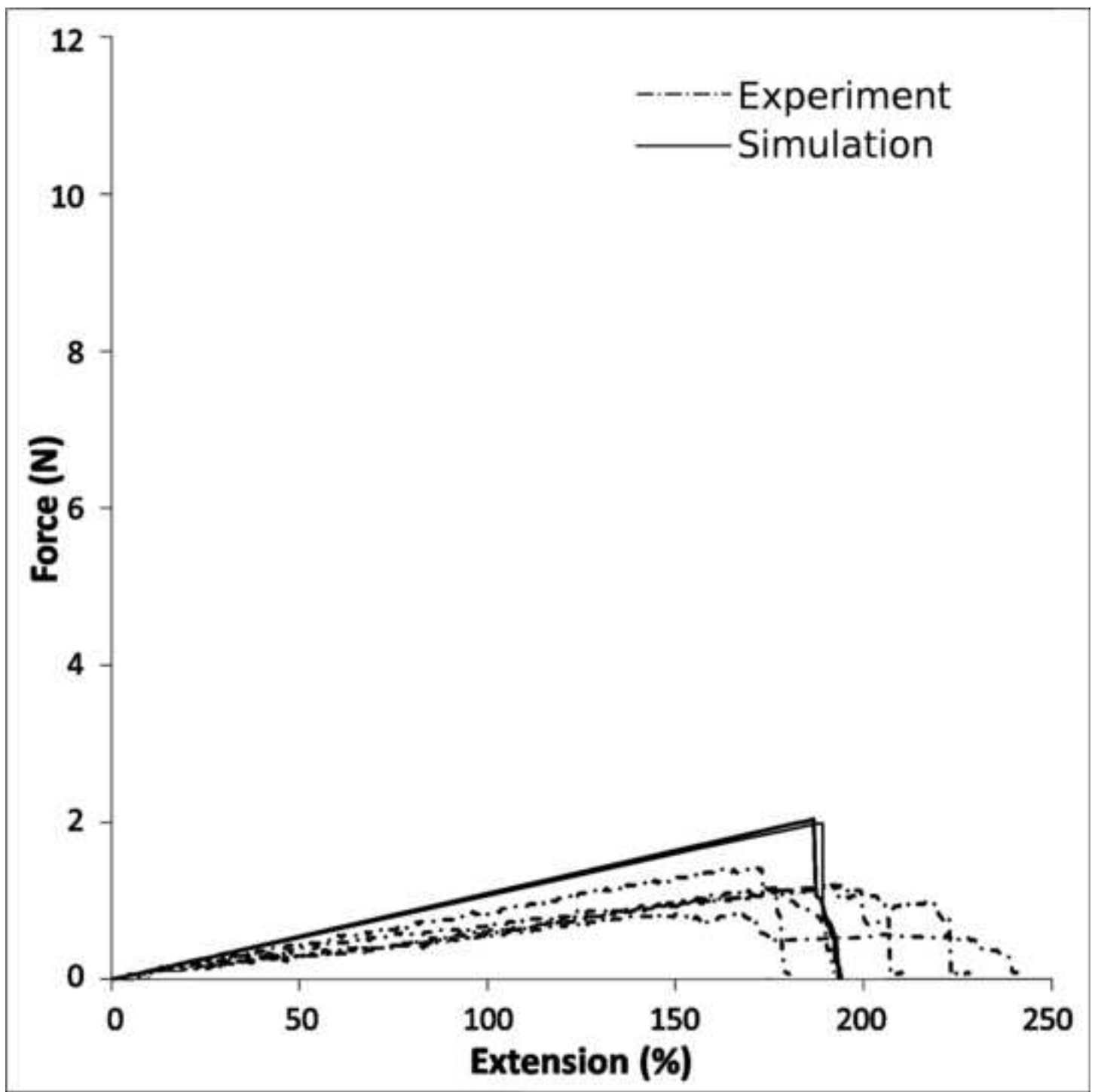


Figure 8 revised
[Click here to download high resolution image](#)

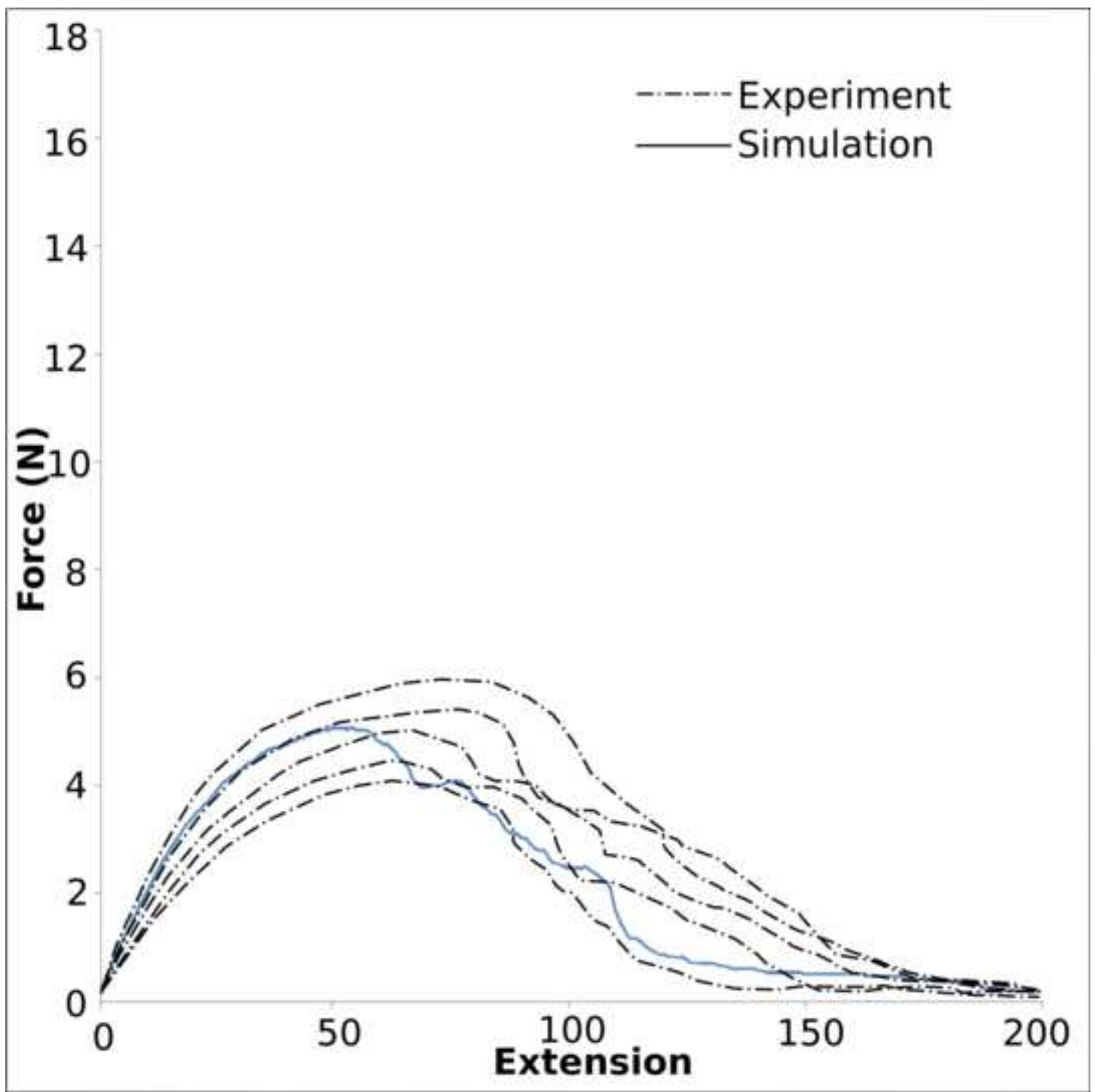


Figure 9a colour
[Click here to download high resolution image](#)

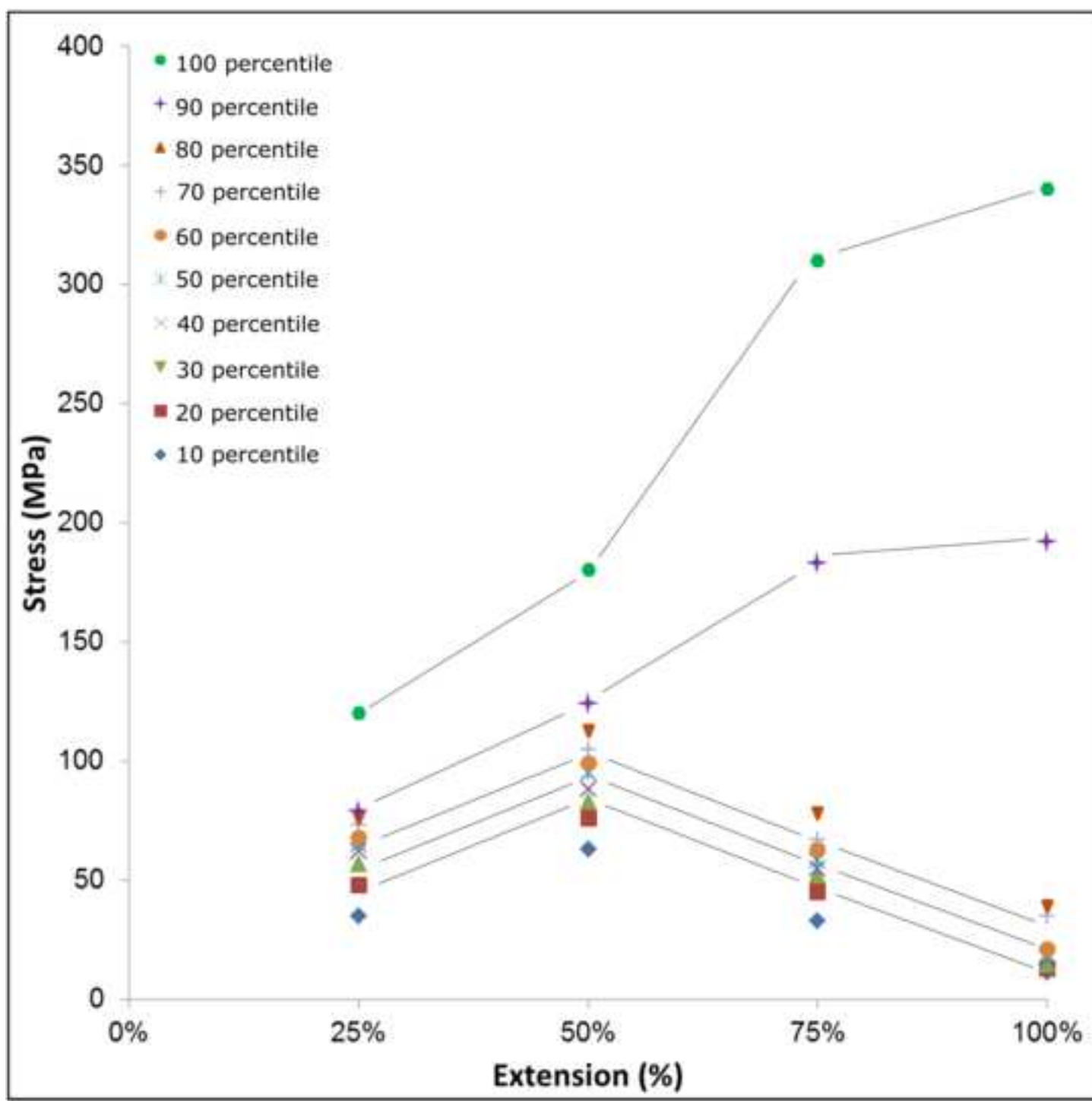


Figure 9a b&w
[Click here to download high resolution image](#)

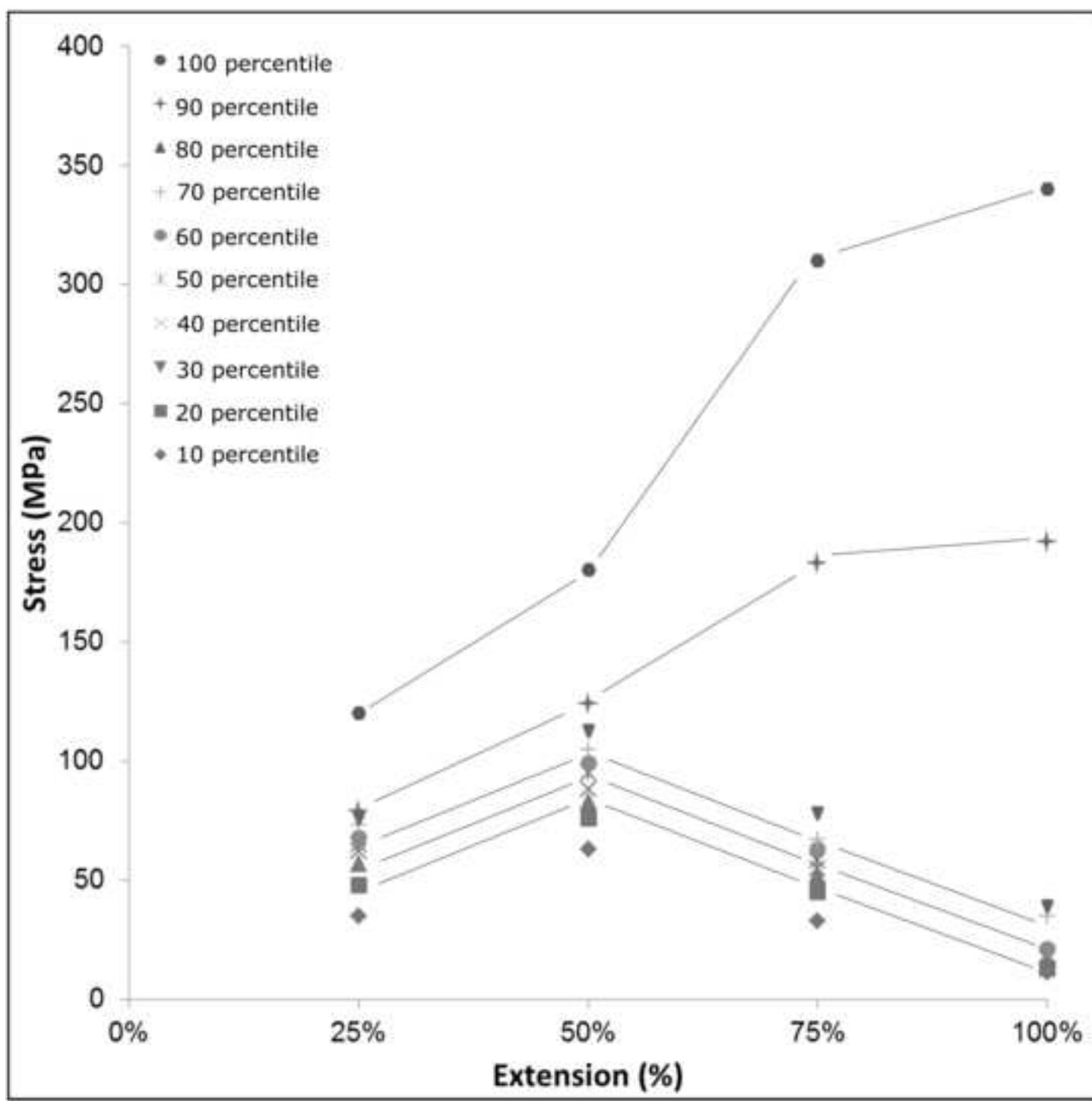


Figure 9b colour
[Click here to download high resolution image](#)

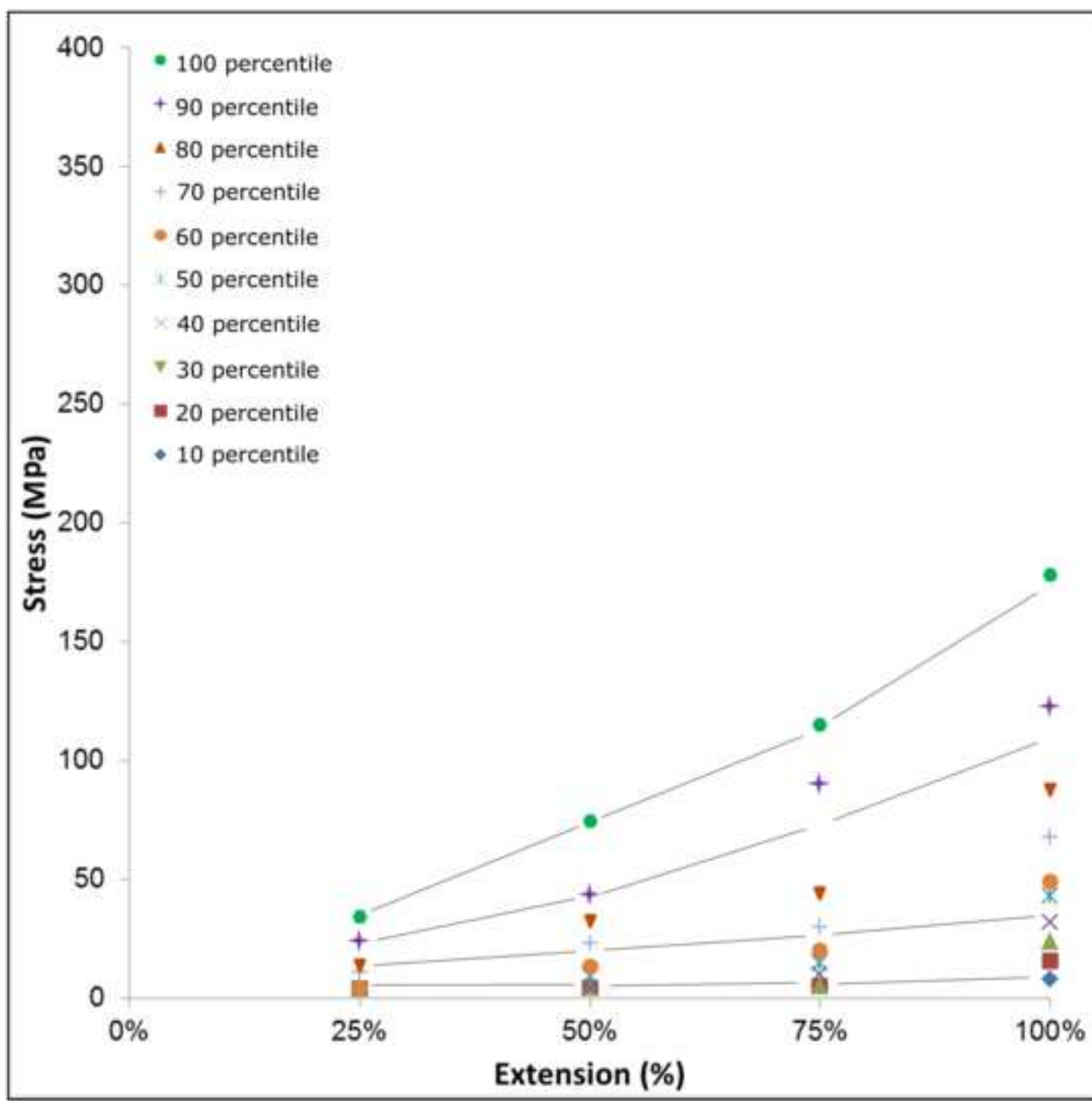


Figure 9b b&w
[Click here to download high resolution image](#)

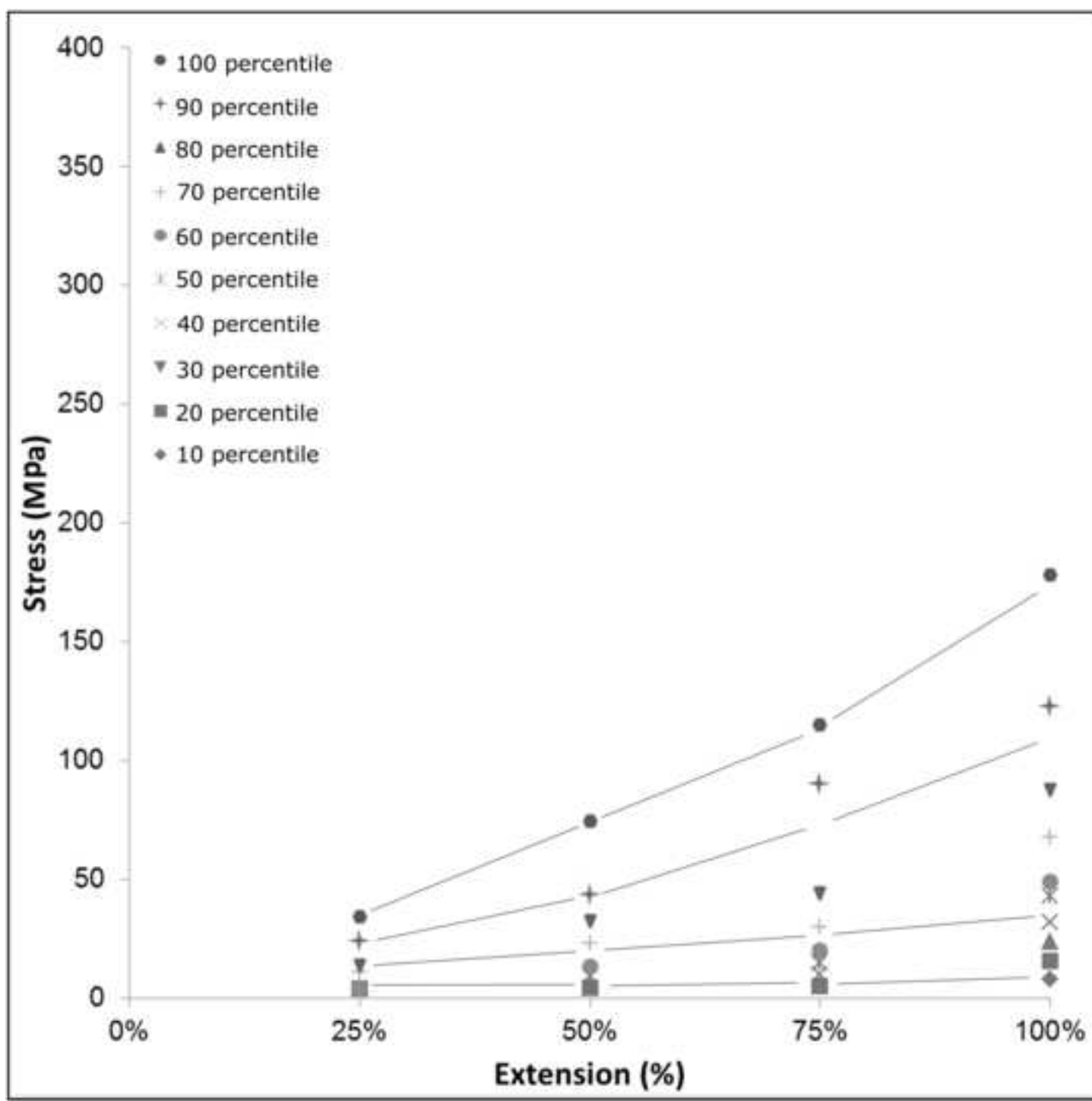


Figure 10 new
[Click here to download high resolution image](#)

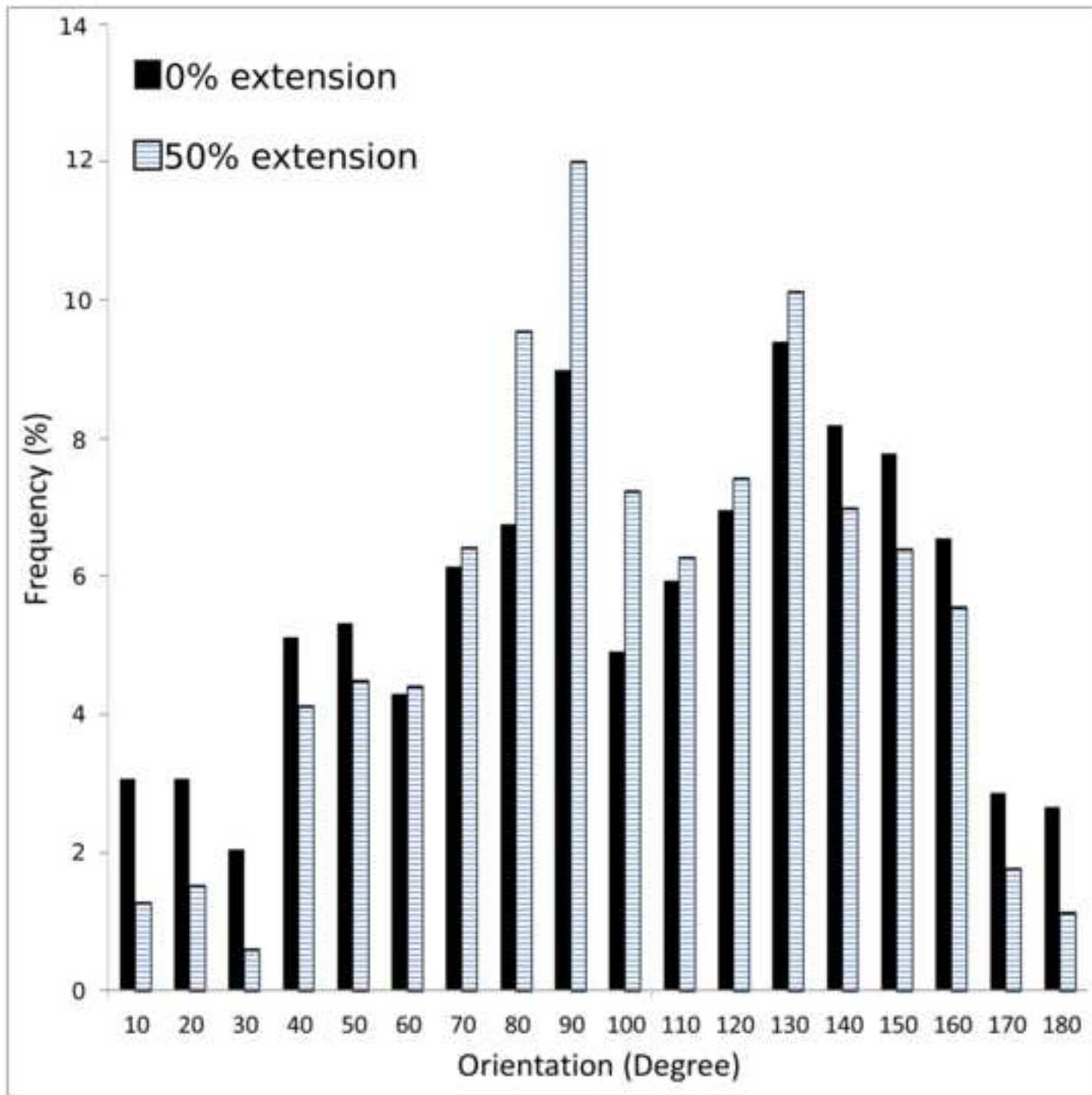


Figure 11 colour
[Click here to download high resolution image](#)

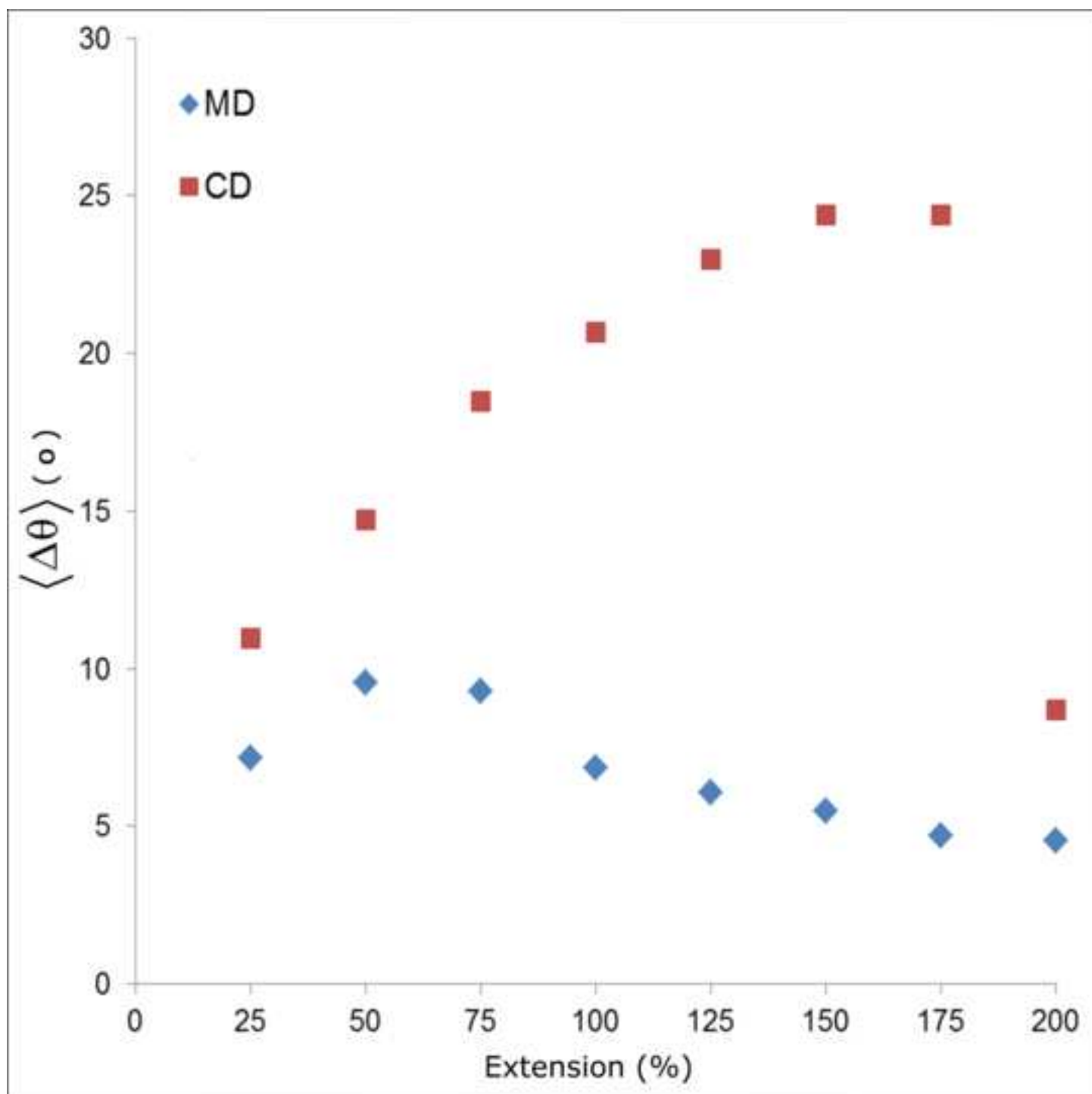


Figure 11 b&w
[Click here to download high resolution image](#)

